

Theoretical study of peristaltic flow in an annulus



By

Nuzhat Irshad

Supervised By

Dr. Sohail Nadeem

Department of Mathematics
Quaid-i-Azam University
Islamabad, Pakistan
2013

Theoretical study of peristaltic flow in an annulus



By
Nuzhat Irshad

A Dissertation submitted in the Partial Fulfillment of the Requirements

For the

Degree of

MASTER OF PHILOSOPHY

IN

MATHEMATICS

Supervised By

Dr. Sohail Nadeem

Department of Mathematics

Quaid-i-Azam University

Islamabad, Pakistan

2013

Theoretical study of peristaltic flow in an annulus


By

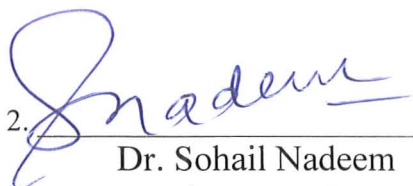
Nuzhat Irshad

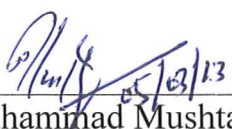
CERTIFICATE

A DISSERTATION SUBMITTED IN THE PARTIAL FULFILLMENT OF THE
REQUIREMENTS FOR THE DEGREE OF THE MASTER OF
PHILOSOPHY

We accept this dissertation as conforming to the required standard

1. 
Dr. Muhammad Ayub
(Chairman)

2. 
Dr. Sohail Nadeem
(Supervisor)

3. 
Dr. Muhammad Mushtaq
(External Examiner)

Department of Mathematics
Quaid-i-Azam University
Islamabad, Pakistan
2013

Acknowledgement

First of all, I would like to thank Almighty Allah who made it possible for me to complete my thesis in time.

Special thanks to my supervisor Dr. SohailNadeemfor the continuous support , motivation, enthusiasm, and immense knowledge .His encouragement and efforts helped me to undertake this work. I could not have imagined having a better advisor and mentor for my M.phil study.

I would like to pay my gratitude to my parents and my brothers for supporting me spiritually throughout my life. Last but not the least, my friends had been enlightmentspeciallyAsma, Afshan, Ambreen, Anums, Maryam,Saminas, Shumaila, Sapna and Mona for their moral support and unconditional love and concern.

Preface

During the past many years the study of Peristaltic flows of Newtonian and non-Newtonian fluids have achieved lot of importance due to its technologies and physiologist applications. Some typical applications of such flows are urine from kidney to bladder, swallowing food bolus towards the esophagus, chime motion in the gastrointestinal tract, vasomotion of small blood vessels and motion of spermatozoa in human reproductive tract. Peristaltic transport of a toxic liquid is utilized in nuclear reactor to retrieve permeation of the outside environment. Several studies are reported regarding the peristaltic flows of Newtonian and non-Newtonian fluids keeping different flow geometries.

In the above studies the concept of induced magnetic field is taken into account. There are only few studies in literature which discuss the peristaltic flows of Newtonian and non-Newtonian fluids with induced magnetic field effects. Actually when we consider the effects of induced magnetic field number of equations will increase and become complicated which are very difficult to solve. Some recent studies on the topic are given in the refs[1-7]. Keeping in mind the above importance, the dissertation is arranged as follows:

In chapter one, we have examined the peristaltic flow of a nanofluid in a uniform tube with induced magnetic field. The problem is simplified by using the approximations of long wavelength and low Reynolds number and then solved by using HPM (homotopy perturbation method) and exact solution method. The expressions for velocity, stream function, pressure rise, induced magnetic field and current density are computed and discussed through graphs.

Chapter two is devoted to the study of the peristaltic flow of a hyperbolic tangent fluid in a uniform tube with induced magnetic field. The problem is simplified by using the approximation of long wavelength and then solved by using HPM (homotopy perturbation method) and exact solution methods. The expression for velocity, stream function, pressure rise, induced magnetic field and current density are computed and discussed through graphs.

Contents

1 Influence of induced magnetic field on peristaltic flow of nanofluid in an annulus	3
1.1 Introduction	3
1.2 Mathematical formulation	3
1.3 Formulation of the problem	5
1.4 Rate of volume flow and boundary conditions	11
1.5 Solution of the Problem	12
1.5.1 Homotopy Perturbation Solution	12
1.5.2 Zeroth-order problem	13
1.5.3 First-order problem	13
1.5.4 Second-order problem	14
1.5.5 Zeroth-order solution	14
1.5.6 First-order solution	14
1.5.7 Second-order solution	15
1.6 Results and discussion	19
1.6.1 Pumping characteristics	19
1.6.2 Nanoparticle Phenomena	19
1.6.3 Magnetic Field Characteristics	20
1.6.4 Fluid Trapping	20
1.7 Concluding Remarks	31
1.8 Appendix I	33

2	Influence of induced magnetic field on peristaltic flow of hyperbolic tangent fluid in an annulus	35
2.1	Introduction	35
2.2	Basic Equations	35
2.3	Formulation of the Problem	37
2.4	Rate of volume flow and boundary conditions	42
2.5	Solution of the Problem	43
	2.5.1 Homotopy Perturbation Solution	44
2.6	Results and Discussion	48
	2.6.1 Pumping Characteristics	48
	2.6.2 Magnetic Field Characteristics	49
	2.6.3 Fluid Trapping	49
2.7	Concluding Remarks	63
2.8	Appendix II	65

Chapter 1

Influence of induced magnetic field on peristaltic flow of nanofluid in an annulus

1.1 Introduction

This chapter looks at the peristaltic flow of nanofluid in an annulus. The flow is investigated in a wave frame of reference moving with velocity of the wave c . Temperature and nanoparticle equations have been solved analytically by using Homotopy Perturbation Method while exact solutions have been calculated for velocity, axial induced magnetic field, current distribution, pressure gradient and stream functions. The effects of various emerging parameters are investigated for sinusoidal wave. The phenomena of trapping has also been discussed at the end of chapter.

1.2 Mathematical formulation

The basic equations of magnetohydrodynamics, neglecting the displacement currents and free charges, are defined as [1]

(i) Maxwell's equation

$$\nabla \cdot \mathbf{H}'^+ = 0 , \quad (1.1)$$

$$\nabla \cdot \mathbf{E}' = 0, \quad (1.2)$$

$$\nabla \times \mathbf{H}'^+ = \mathbf{J}' \quad \text{with } \mathbf{J}' = \sigma \{ \mathbf{E}' + \mu_e (\mathbf{V}' \times \mathbf{H}'^+) \}, \quad (1.3)$$

$$\nabla \times \mathbf{E}' = -\mu_e \frac{\partial \mathbf{H}'^+}{\partial t'}, \quad (1.4)$$

(ii) The continuity equation

$$\nabla \cdot \mathbf{V}' = 0, \quad (1.5)$$

(iii) The Navier-Stokes equation

$$\rho \frac{\mathbf{D}\mathbf{V}'}{\mathbf{D}t'} = -\nabla \tilde{p}' + \nabla \cdot \tilde{\boldsymbol{\tau}}' + \mu_e (\mathbf{J}' \times \mathbf{H}'^+) + \rho \mathbf{f}, \quad (1.6)$$

where \mathbf{V}' is the velocity vector, \mathbf{J}' is the electric current density, \mathbf{E}' is an induced electric field, μ_e is the magnetic permeability while σ is the electrical conductivity and $\mathbf{D}/\mathbf{D}t'$ denotes the material derivative and $\tilde{\boldsymbol{\tau}}'$ is the stress tensor.

(iv) The energy equation

$$(\rho c)_f \frac{\mathbf{D}\tilde{\mathbb{T}}}{\mathbf{D}t'} = k \nabla^2 \tilde{\mathbb{T}} + (\rho c)_p [d_b \nabla \tilde{\mathbb{C}} \cdot \nabla \tilde{\mathbb{T}} + (\frac{d_{\tilde{\mathbb{T}}}}{\tilde{\mathbb{T}}_1}) \nabla \tilde{\mathbb{T}} \cdot \nabla \tilde{\mathbb{T}}], \quad (1.7)$$

(v) The mass concentration

$$\frac{\mathbf{D}\tilde{\mathbb{C}}}{\mathbf{D}t'} = d_b \nabla^2 \tilde{\mathbb{C}} + (\frac{d_{\tilde{\mathbb{T}}}}{\tilde{\mathbb{T}}_1}) \nabla^2 \tilde{\mathbb{T}}, \quad (1.8)$$

where $\tilde{\mathbb{T}}$ and $\tilde{\mathbb{C}}$ represent the nanoparticle phenomenon, d_b the Brownian diffusion coefficient and $d_{\tilde{\mathbb{T}}}$ the thermophoretic diffusion coefficient.

(iv) On combining Maxwell's equations, we get induction equation as follow

$$\frac{\partial \mathbf{H}'^+}{\partial t'} = \nabla \times \{ \mathbf{V}' \times \mathbf{H}'^+ \} + \zeta \nabla^2 \mathbf{H}'^+. \quad (1.9)$$

where magnetic diffusivity is given as $\zeta = \frac{1}{\sigma \mu_e}$.

1.3 Formulation of the problem

Consider unsteady flow of incompressible and electrically conducting nanofluid through the gap between two coaxial tubes. The inner tube is uniform and rigid, and sustained at temperature \tilde{T}_0 and nanoparticle velocity \tilde{C}_0 while outer tube has a sinusoidal wave travelling down its walls having temperature \tilde{T}_1 and nanoparticle velocity \tilde{C}_1 . We choose cylindrical coordinates (R', Z') such that R' is the radial coordinates and Z' is the axial coordinate. An external uniform magnetic field of strength $H_0 R'_2 / R'$ is applied radially which will give rise to an induced magnetic field $\mathbf{H}' (h'_{R'}(R', Z', t'), 0, h'_{z'}(R', Z', t'))$ and total magnetic field will be $\mathbf{H}^+ \left(\frac{H_0 R'_2}{R'} + h'_{R'}, 0, h'_{z'} \right)$.

The stress tensor for viscous fluid is given as

$$\tilde{\tau}' = \mu (\text{grad } \mathbf{V}' + (\text{grad } \mathbf{V}')^T). \quad (1.10)$$

The walls of the tubes are assumed to be non-conductive and geometry of the walls surface is illustrated in Fig(1.1)

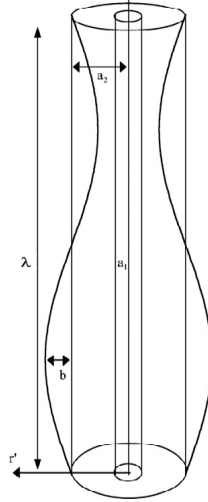


Fig.(1.1) Geometry of the problem

$$R'_1 = a_1, \quad (1.11)$$

$$R'_2 = a_2 + b \sin \frac{2\pi}{\lambda} (Z' - ct'), \quad (1.12)$$

where a_1 , a_2 are the radius of the inner and outer tubes, b is the amplitude of the wave, λ is the wavelength, c is the propagation velocity and t' is the time.

By assuming the flow parameters independent of the azimuthal coordinates, the velocity takes the form $\mathbf{V}' = (\tilde{U}', 0, \tilde{W}')$ where \tilde{U}' and \tilde{W}' are the velocity components in R' and Z' direction, respectively. Temperature, and concentration fields take the form

$$\tilde{\mathbb{T}} = \tilde{\mathbb{T}}(R', Z', t'), \quad \tilde{\mathbb{C}} = \tilde{\mathbb{C}}(R', Z', t'). \quad (1.13)$$

The governing equations along with nanoparticles in the fixed frame are given as

$$\frac{\partial h'_R}{\partial R'} + \frac{h'_{R'}}{R'} + \frac{\partial h'_{Z'}}{\partial Z'} = 0, \quad (1.14)$$

$$\frac{\partial \tilde{U}'}{\partial R'} + \frac{\tilde{U}'}{R'} + \frac{\partial \tilde{W}'}{\partial Z'} = 0, \quad (1.15)$$

$$\begin{aligned} \rho \left(\frac{\partial \tilde{U}'}{\partial t'} + \tilde{U}' \frac{\partial \tilde{U}'}{\partial R'} + \tilde{W}' \frac{\partial \tilde{U}'}{\partial Z'} \right) &= -\frac{\partial \tilde{p}'}{\partial R'} + \frac{1}{R'} \frac{\partial (R' \tilde{\tau}_{RR})}{\partial R'} + \frac{\partial (\tilde{\tau}_{RZ})}{\partial Z'} - \frac{\tilde{\tau}_{\theta\theta}}{R'} \\ &+ \mu_e h'_{Z'} \left[\frac{\partial}{\partial Z'} \left(H'_o \frac{R'_2}{R'} + h'_{R'} \right) - \frac{\partial h'_{Z'}}{\partial R'} \right], \end{aligned} \quad (1.16)$$

$$\begin{aligned} \rho \left(\frac{\partial \tilde{U}'}{\partial t'} + \tilde{U}' \frac{\partial \tilde{W}'}{\partial R'} + \tilde{W}' \frac{\partial \tilde{W}'}{\partial Z'} \right) &= -\frac{\partial \tilde{p}'}{\partial Z'} + \frac{1}{R'} \frac{\partial (R' \tilde{\tau}_{RZ})}{\partial R'} + \frac{\partial (\tilde{\tau}_{ZZ})}{\partial Z'} \\ &+ \mu_e \left[\frac{\partial h'_{Z'}}{\partial R'} - \frac{\partial}{\partial Z'} \left(H'_o \frac{R'_2}{R'} + h'_{R'} \right) \right] \left(H'_o \frac{R'_2}{R'} + h'_{R'} \right) + \rho g \alpha_{\tilde{\mathbb{T}}} (\tilde{\mathbb{T}} - \tilde{\mathbb{T}}_1) \\ &+ \rho g \alpha_{\tilde{\mathbb{C}}} (\tilde{\mathbb{C}} - \tilde{\mathbb{C}}_1). \end{aligned} \quad (1.17)$$

Energy and mass concentration equations are defined as

$$\begin{aligned}
(\tilde{U}' \frac{\partial \tilde{T}}{\partial R'} + \tilde{W}' \frac{\partial \tilde{T}}{\partial Z'}) = & \alpha_2 \left(\frac{\partial^2 \tilde{T}}{\partial R'^2} + \frac{1}{R'} \frac{\partial \tilde{T}}{\partial R'} + \frac{\partial^2 \tilde{T}}{\partial Z'^2} \right) + \tau_1 \left\{ d_b \left(\frac{\partial \tilde{C}}{\partial R'} \frac{\partial \tilde{T}}{\partial R'} + \frac{\partial \tilde{C}}{\partial Z'} \frac{\partial \tilde{T}}{\partial Z'} \right) \right. \\
& \left. + \frac{d_T}{\tilde{T}_1} \left[\left(\frac{\partial \tilde{T}}{\partial R'} \right)^2 + \left(\frac{\partial \tilde{T}}{\partial Z'} \right)^2 \right] \right\}, \tag{1.18}
\end{aligned}$$

$$(\tilde{U}' \frac{\partial \tilde{C}}{\partial R'} + \tilde{W}' \frac{\partial \tilde{C}}{\partial Z'}) = d_b \left(\frac{\partial^2 \tilde{C}}{\partial R'^2} + \frac{1}{R'} \frac{\partial \tilde{C}}{\partial R'} + \frac{\partial^2 \tilde{C}}{\partial Z'^2} \right) + \frac{d_T}{\tilde{T}_1} \left(\frac{\partial^2 \tilde{T}}{\partial R'^2} + \frac{1}{R'} \frac{\partial \tilde{T}}{\partial R'} + \frac{\partial^2 \tilde{T}}{\partial Z'^2} \right), \tag{1.19}$$

in the above equations, \tilde{C} is the nanoparticle volume fraction, d_T the thermophoretic diffusion coefficient, d_b the Brownian diffusion coefficients of mass diffusivity $\tau_1 = \frac{(\rho c)_p}{(\rho c)_f}$ depicts the ratio of the effective heat capacity in the case of nanoparticle material and heat capacity of the fluid, and the magnetic induction equations in component form is given as

$$\begin{aligned}
\left[\frac{\partial}{\partial t'} + (\tilde{U}' \frac{\partial}{\partial R'} + \tilde{W}' \frac{\partial}{\partial Z'}) - \frac{\partial \tilde{U}'}{\partial R'} \right] \left(H'_o \frac{R'_2}{R'} + h'_R \right) - \frac{\partial \tilde{U}'}{\partial R'} h'_Z \\
= \zeta \frac{\partial}{\partial Z'} \left[\left(\frac{\partial}{\partial Z'} \left(H'_o \frac{R'_2}{R'} + h'_R \right) \right) - \left(\frac{\partial h'_Z}{\partial R'} \right) \right], \tag{1.20}
\end{aligned}$$

$$\begin{aligned}
\left[\frac{\partial}{\partial t'} + (\tilde{U}' \frac{\partial}{\partial R'} + \tilde{W}' \frac{\partial}{\partial Z'}) - \frac{\partial \tilde{W}'}{\partial Z'} \right] h'_z - \frac{\partial \tilde{W}'}{\partial R'} \left(H'_o \frac{R'_2}{R'} + h'_R \right) \\
= \zeta \left[\frac{1}{R'} \frac{\partial}{\partial R'} \left(R' \frac{\partial h'_Z}{\partial R'} \right) - \frac{\partial}{\partial Z'} \left(\frac{\partial}{\partial R'} + \frac{1}{R'} \right) \left(H'_o \frac{R'_2}{R'} + h'_R \right) \right]. \tag{1.21}
\end{aligned}$$

In the fixed coordinates (R', Z') , the flow between the two cylinders is unsteady. It converts steady in a wave structure (r', z') moving with similar speed as the wave movement in the Z' direction. Both structures are connected through the following transformations

$$r' = R', \quad z' = Z' - ct', \quad \tilde{U}' = u', \quad \tilde{W}' = w' - ct', \tag{1.22}$$

where u' , w' are the velocity components in the wave structure. Suitable boundary limits in wave structures stands

$$\begin{aligned} w' &= -c, \text{ at } r' = r'_1, h'_z = 0, h'_{r'} = 0, \\ w' &= -c, \text{ at } r' = r'_2 = a_2 + b \sin \frac{2\pi}{\lambda}(z'), \end{aligned} \quad (1.23)$$

$$\tilde{\mathbb{T}} = \tilde{\mathbb{T}}_0 \text{ at } r' = r'_1, \tilde{\mathbb{T}} = \tilde{\mathbb{T}}_1 \text{ at } r' = r'_2, \quad (1.24)$$

$$\tilde{\mathbb{C}} = \tilde{\mathbb{C}}_0 \text{ at } r' = r'_1, \tilde{\mathbb{C}} = \tilde{\mathbb{C}}_1 \text{ at } r' = r'_2. \quad (1.25)$$

Introducing the dimensionless parameters

$$\begin{aligned} \mathbb{R} &= \frac{R'}{a_2}, \mathbb{r} = \frac{r'}{a_2}, \mathbb{Z} = \frac{Z'}{\lambda}, \mathbb{z} = \frac{z'}{\lambda}, \mathbb{W} = \frac{\tilde{W}'}{c}, \mathbb{w} = \frac{w'}{c}, \mathbb{U} = \frac{\lambda \tilde{U}'}{a_2 c}, \mathbb{u} = \frac{\lambda u'}{a_2 c}, \\ \mathbb{P} &= \frac{a_2^2 p'}{c \lambda \mu}, \theta = \frac{\tilde{\mathbb{T}} - \tilde{\mathbb{T}}_1}{\tilde{\mathbb{T}}_0 - \tilde{\mathbb{T}}_1}, \mathbb{t} = \frac{ct'}{\lambda}, \hat{\delta} = \frac{a_2}{\lambda}, \mathbb{R}_y = \frac{\rho c a_2}{\mu}, \sigma = \frac{\tilde{\mathbb{C}} - \tilde{\mathbb{C}}_1}{\tilde{\mathbb{C}}_0 - \tilde{\mathbb{C}}_1}, \\ \mathbb{r}_1 &= \frac{r'_1}{a_2} = \epsilon, \mathbb{r}_2 = \frac{r'_2}{H_2} = 1 + \alpha \sin 2\pi z, \epsilon = \frac{a_1}{a_2}, h_r = \frac{h'_r}{H_0}, h_z = \frac{h'_z}{H_0}, \\ g_r &= \frac{\rho g \alpha \tilde{\mathbb{T}} H_2^2 (\tilde{\mathbb{T}}_0 - \tilde{\mathbb{T}}_1)}{c \mu}, b_r = \frac{\rho g \alpha \tilde{\mathbb{C}} H_2^2 (\tilde{\mathbb{C}}_0 - \tilde{\mathbb{C}}_1)}{c \mu}, N_b = \frac{(\rho c)_p d_b (\tilde{\mathbb{C}}_0 - \tilde{\mathbb{C}}_1)}{(\rho c)_f \alpha_2}, \\ N_t &= \frac{(\rho c)_p d_{\tilde{\mathbb{T}}} (\tilde{\mathbb{T}}_0 - \tilde{\mathbb{T}}_1)}{(\rho c)_f \tilde{\mathbb{T}}_1 \alpha_2}, P_r = \frac{\eta c_p}{k}, \alpha_2 = \frac{k}{(\rho c)_f}. \end{aligned} \quad (1.26)$$

We define N_t , b_r , R_y , g_r , N_b , $\hat{\delta}$, α , ϵ are the thermophoresis parameter, local nanoparticle Grashof number, Reynolds number, local temperature Grashof number, Brownian motion parameter, wave number, α is the amplitude ratio and ϵ is radius ratio respectively.

Making use of above non-dimensional parameters Eqs.(1.14) to (1.21) along with conditions (1.23) to (1.25) take the form

$$\frac{\partial h_r}{\partial \mathbb{r}} + \frac{h_r}{\mathbb{r}} + \hat{\delta} \frac{\partial h_z}{\partial \mathbb{z}} = 0, \quad (1.27)$$

$$\frac{\partial \mathbb{u}}{\partial \mathbb{r}} + \frac{\mathbb{u}}{\mathbb{r}} + \frac{\partial \mathbb{w}}{\partial \mathbb{z}} = 0, \quad (1.28)$$

$$\hat{\delta}^3 R_y \left(u \frac{\partial u}{\partial r} + w \frac{\partial u}{\partial z} \right) = -\frac{\partial p}{\partial r} + \hat{\delta}^2 \frac{\partial}{\partial z} (\tau_{rz}) + \frac{\hat{\delta}}{r} \frac{\partial}{\partial r} (r \tau_{rr}) - \frac{\hat{\delta}}{r} \tau_{\theta\theta} + S^2 R_y \left[\hat{\delta} \left(\frac{1}{r} \frac{\partial r_2}{\partial z} + \frac{\partial h_r}{\partial r} \right) - \frac{\partial h_z}{\partial r} h_z \right], \quad (1.29)$$

$$\hat{\delta} R_y \left(u \frac{\partial w}{\partial r} + w \frac{\partial w}{\partial z} \right) = -\frac{\partial p}{\partial z} + \frac{1}{r} \frac{\partial}{\partial r} (r \tau_{rz}) + \hat{\delta} \frac{\partial}{\partial z} (\tau_{zz}) + S^2 R_y \left[\frac{\partial h_z}{\partial r} - \hat{\delta} \left(\frac{1}{r} \frac{\partial r_2}{\partial z} + \frac{\partial h_r}{\partial r} \right) \right] \left(\frac{r_2}{r} + h_r \right) + g_r \theta + b_r \sigma, \quad (1.30)$$

where

$$\begin{aligned} \tau_{rr} &= 2 \frac{\partial u}{\partial r}, \\ \tau_{rz} &= \left(\frac{\partial u}{\partial z} \hat{\delta}^2 + \frac{\partial w}{\partial r} \right), \\ \tau_{zz} &= 2 \frac{\partial w}{\partial z}, \\ \tau_{\theta\theta} &= 2 \frac{u}{r}. \end{aligned} \quad (1.31)$$

Energy, mass and induction equations become

$$\begin{aligned} \hat{\delta} a_2 c \left[u \frac{\partial \tilde{T}}{\partial r} + w \frac{\partial \tilde{T}}{\partial z} \right] &= \alpha_2 \left(\frac{\partial^2 \tilde{T}}{\partial r^2} + \frac{1}{r} \frac{\partial \tilde{T}}{\partial r} + \hat{\delta}^2 \frac{\partial^2 \tilde{T}}{\partial z^2} \right) + \tau_1 \left\{ d_b \left(\frac{\partial \tilde{C}}{\partial r} \frac{\partial \tilde{T}}{\partial r} + \hat{\delta}^2 \frac{\partial \tilde{C}}{\partial z} \frac{\partial \tilde{T}}{\partial z} \right) \right. \\ &\quad \left. + \frac{d_{T_1}}{\tilde{T}_1} \left[\left(\frac{\partial \tilde{T}}{\partial r} \right)^2 + \hat{\delta}^2 \left(\frac{\partial \tilde{T}}{\partial z} \right)^2 \right] \right\}, \end{aligned} \quad (1.32)$$

$$\hat{\delta} a_2 c \left[u \frac{\partial \tilde{C}}{\partial r} + w \frac{\partial \tilde{C}}{\partial z} \right] = d_b \left(\frac{\partial^2 \tilde{C}}{\partial r^2} + \frac{1}{r} \frac{\partial \tilde{C}}{\partial r} + \hat{\delta}^2 \frac{\partial^2 \tilde{C}}{\partial z^2} \right) + \frac{d_{T_1}}{\tilde{T}_1} \left(\frac{\partial^2 \tilde{T}}{\partial r^2} + \frac{1}{r} \frac{\partial \tilde{T}}{\partial r} + \hat{\delta}^2 \frac{\partial^2 \tilde{T}}{\partial z^2} \right), \quad (1.33)$$

$$\hat{\delta} \left[\frac{\partial}{\partial t} + \left(u \frac{\partial}{\partial r} + w \frac{\partial}{\partial z} \right) - \frac{\partial u}{\partial r} \right] \left(\frac{r_2}{r} + h_r \right) - \hat{\delta} \frac{\partial u}{\partial r} h_z = \frac{\hat{\delta}}{R_m} \frac{\partial}{\partial z} \left[\hat{\delta} \left(\frac{1}{r} \frac{\partial r_2}{\partial z} + \frac{\partial h_r}{\partial z} \right) - \frac{\partial h_z}{\partial r} \right], \quad (1.34)$$

$$\hat{\delta} \left[\frac{\partial}{\partial t} + \left(u \frac{\partial}{\partial r} + w \frac{\partial}{\partial z} \right) - \frac{\partial w}{\partial z} \right] h_z - \frac{\partial w}{\partial r} \left(\frac{r_2}{r} + h_r \right) = \frac{1}{R_m} \left[\frac{1}{r} \frac{\partial}{\partial r} \left(r \frac{\partial h_z}{\partial r} \right) - \hat{\delta} \frac{\partial}{\partial z} \left(\frac{\partial}{\partial r} + \frac{1}{r} \right) \left(\frac{r_2}{r} + h_r \right) \right]. \quad (1.35)$$

Using the long wavelength approximation and dropping terms of order $\hat{\delta}$ and higher, it follows from Eqs. (1.27) to (1.35) that the appropriate equations describing the flow are

$$\frac{\partial h_r}{\partial r} + \frac{h_r}{r} = 0, \quad (1.36)$$

$$\frac{\partial u}{\partial r} + \frac{u}{r} + \frac{\partial w}{\partial z} = 0, \quad (1.37)$$

$$\frac{\partial p}{\partial r} = 0, \quad (1.38)$$

$$\frac{\partial p}{\partial z} = \frac{1}{r} \frac{\partial}{\partial r} \left(r \frac{\partial w}{\partial z} \right) + S^2 R_y \frac{\partial h_z}{\partial r} \left(\frac{r_2}{r} + h_r \right) + g_r \theta + b_r \sigma, \quad (1.39)$$

$$\frac{1}{r} \frac{\partial}{\partial r} \left(r \frac{\partial \theta}{\partial r} \right) + N_b \frac{\partial \sigma}{\partial r} \frac{\partial \theta}{\partial r} + N_t \left(\frac{\partial \theta}{\partial r} \right)^2 = 0, \quad (1.40)$$

$$\left(\frac{1}{r} \frac{\partial}{\partial r} \left(r \frac{\partial \sigma}{\partial r} \right) \right) + \frac{N_t}{N_b} \left(\frac{1}{r} \frac{\partial}{\partial r} \left(r \frac{\partial \theta}{\partial r} \right) \right) = 0, \quad (1.41)$$

$$\frac{\partial w}{\partial r} \left(\frac{r_2}{r} + h_r \right) = - \frac{1}{R_m} \left[\frac{1}{r} \frac{\partial}{\partial r} \left(r \frac{\partial h_z}{\partial r} \right) \right], \quad (1.42)$$

where $S^2 = \frac{H_o^2 \mu_e}{\rho c^2}$ and $R_m = \frac{a_2}{\zeta}$ are Strommer's number(magnetic force number) and the magnetic Reynolds number respectively. Eq. (1.38) displays that p is not a function of r .

1.4 Rate of volume flow and boundary conditions

In the fixed coordinates volume flow rate in the instantaneous position is specified by

$$\bar{Q} = 2\pi \int_{R'_1}^{R'_2} R' \widetilde{W} dR', \quad (1.43)$$

where R'_2 is a function of Z' and t' . Invoking Eq. (1.22) into Eq. (1.43) and integrating produces

$$\bar{Q} = \bar{q} + \pi c (r'_2{}^2 - r'_1{}^2), \quad (1.44)$$

where

$$\bar{q} = 2\pi \int_{r'_1}^{r'_2} r' w' dr'. \quad (1.45)$$

In the moving coordinates system the volume flow rate is independent of time as mention in Eq. (1.45). Here r'_2 is the function of z' alone. Using dimensionless variables we find

$$F = \frac{\bar{q}}{\pi a_2^2 c} = 2 \int_{r'_1}^{r'_2} r w dr. \quad (1.46)$$

Over a period $T = \lambda/c$ the time-mean flow at a fixed z position is defined as

$$\theta' = \frac{1}{T} \int_0^T \bar{Q} dt'. \quad (1.47)$$

Invoking Eq. (1.44) into Eq. (1.47) and integrating, we attain

$$\theta' = \bar{q} + \pi c \left(a_2^2 - a_1^2 + \frac{b^2}{2} \right), \quad (1.48)$$

which can be inscribed as

$$\frac{\theta'}{\pi a_2^2 c} = \frac{\tilde{q}}{\pi a_2^2 c} + 1 + \frac{\alpha^2}{2} - \epsilon^2. \quad (1.49)$$

Dimensionless time-mean flow can be defined as

$$\theta = \frac{\theta'}{\pi c a_2^2}. \quad (1.50)$$

With the aid of Eqs. (1.46) and (1.50), Eq. (1.49) takes the form

$$\theta = F + 1 + \frac{\alpha^2}{2} - \epsilon^2. \quad (1.51)$$

The consistent dimensionless boundary conditions for the problem under consideration are defined as

$$\begin{aligned} w &= -1 \text{ at } r = r_1 = \epsilon, \quad w = -1 \text{ at } r = r_2 = 1 + \alpha \sin(2\pi z), \\ h_r &= 0, h_z = 0 \text{ at } r = r_1, \\ \sigma &= 1 \text{ at } r = r_1, \quad \sigma = 0 \quad \text{at } r = r_2, \\ \theta &= 1 \text{ at } r = r_1, \quad \theta = 0 \quad \text{at } r = r_2. \end{aligned} \quad (1.52)$$

1.5 Solution of the Problem

1.5.1 Homotopy Perturbation Solution

To achieve the solution of above equations, we used homotopy perturbation method. The homotopy perturbation method advises that we write Eqs. (1.32) to (1.33), as [15]

$$H(\sigma, x) = (1 - x) [\mathcal{L}(\sigma) - \mathcal{L}(\sigma_{10})] + x \left[\mathcal{L}(\sigma) + \frac{N_t}{N_b} \left(\frac{1}{r} \frac{\partial}{\partial r} \left(r \frac{\partial \theta}{\partial r} \right) \right) \right], \quad (1.53)$$

$$H(\theta, x) = (1 - x) [\mathcal{L}(\theta) - \mathcal{L}(\theta_{10})] + x \left[\mathcal{L}(\theta) + N_b \frac{\partial \theta}{\partial r} \frac{\partial \sigma}{\partial r} + N_t \left(\frac{\partial \theta}{\partial r} \right)^2 \right], \quad (1.54)$$

or

$$H(\sigma, x) = \mathcal{L}(\sigma) - \mathcal{L}(\sigma_{10}) + x \mathcal{L}(\sigma_{10}) + x \left[\frac{N_t}{N_b} \left(\frac{1}{r} \frac{\partial}{\partial r} \left(r \frac{\partial \theta}{\partial r} \right) \right) \right], \quad (1.55)$$

$$H(\theta, x) = \mathcal{L}(\theta) - \mathcal{L}(\theta_{10}) + x \mathcal{L}(\theta_{10}) + x \left[N_b \frac{\partial \theta}{\partial r} \frac{\partial \sigma}{\partial r} + N_t \left(\frac{\partial \theta}{\partial r} \right)^2 \right]. \quad (1.56)$$

The linear operator and the initial guesses are chosen as

$$\begin{aligned}\mathcal{L}_{\theta_r} &= \frac{1}{r} \frac{\partial}{\partial r} \left(r \frac{\partial}{\partial r} \right), \quad \mathcal{L}_{\sigma_r} = \frac{1}{r} \frac{\partial}{\partial r} \left(r \frac{\partial}{\partial r} \right), \\ \sigma_{10}(r, z) &= \left(\frac{r - r_2}{r_1 - r_2} \right), \quad \theta_{10}(r, z) = \left(\frac{r - r_2}{r_1 - r_2} \right).\end{aligned}\tag{1.57}$$

According to HPM, we define

$$\begin{aligned}\theta &= \theta_0 + x\theta_1 + x^2\theta_2 + \dots, \\ \sigma &= \sigma_0 + x\sigma_1 + x^2\sigma_2 + \dots\end{aligned}\tag{1.58}$$

With the help of above equations, Eqs. (1.55) and (1.56) after equating the like powers of x give the following systems.

1.5.2 Zeroth-order problem

$$\begin{aligned}\mathcal{L}(\sigma_0) - \mathcal{L}(\sigma_{10}) &= 0, \\ \mathcal{L}(\theta_0) - \mathcal{L}(\theta_{10}) &= 0,\end{aligned}\tag{1.59}$$

$$\begin{aligned}\theta_0 = \sigma_0 &= 1 \text{ at } r = r_1, \\ \theta_0 = \sigma_0 &= 0 \text{ at } r = r_2 = 1 + \alpha \sin 2\pi z.\end{aligned}\tag{1.60}$$

1.5.3 First-order problem

$$\begin{aligned}\mathcal{L}(\sigma_1) &= -\mathcal{L}(\sigma_{10}) - \frac{N_t}{N_b} \left(\frac{1}{r} \frac{\partial}{\partial r} \left(r \frac{\partial \theta_0}{\partial r} \right) \right), \\ \mathcal{L}(\theta_1) &= -\mathcal{L}(\theta_{10}) - N_b \frac{\partial \sigma_0}{\partial r} \frac{\partial \theta_0}{\partial r} - N_t \left(\frac{\partial \theta_0}{\partial r} \right)^2,\end{aligned}\tag{1.61}$$

$$\begin{aligned}\theta_1 &= \sigma_1 = 0 \text{ at } r = r_1, \\ \theta_1 &= \sigma_1 = 0 \text{ at } r = r_2 = 1 + \alpha \sin 2\pi z.\end{aligned}\tag{1.62}$$

1.5.4 Second-order problem

$$\begin{aligned}\mathcal{L}(\sigma_2) &= -\frac{N_t}{N_b} \left(\frac{1}{r} \frac{\partial}{\partial r} \left(r \frac{\partial \theta_1}{\partial r} \right) \right), \\ \mathcal{L}(\theta_2) &= -B_m \left(\frac{\partial \theta_1}{\partial r} \frac{\partial \sigma_0}{\partial r} + \frac{\partial \theta_0}{\partial r} \frac{\partial \sigma_1}{\partial r} \right) - 2N_t \frac{\partial \theta_0}{\partial r} \frac{\partial \theta_1}{\partial r},\end{aligned}\tag{1.63}$$

$$\theta_2 = \sigma_2 = 0 \text{ at } r = r_1,$$

$$\theta_2 = \sigma_2 = 0 \text{ at } r = r_2 = 1 + \alpha \sin 2\pi z,\tag{1.64}$$

We can write the solutions of these problems as

1.5.5 Zeroth-order solution

The zeroth order solution is defined as

$$\begin{aligned}\theta_0(r) &= \left(\frac{r - r_2}{r_1 - r_2} \right), \\ \sigma_0(r) &= \left(\frac{r - r_2}{r_1 - r_2} \right).\end{aligned}\tag{1.65}$$

1.5.6 First-order solution

With the help of expression (1.65), solution of first order system (1.61) subject to boundary condition (1.62) is directly defined as

$$\begin{aligned}\theta_1(r) &= -r^2 b_{12} - \frac{r}{b_1} + b_7 \ln(r) + b_{13}, \\ \sigma_1(r) &= r b_{16} + b_{14} \ln(r) + b_{17} + b_{15}.\end{aligned}\tag{1.66}$$

1.5.7 Second-order solution

Making use of zeroth and first order solution, the solution of second order problem is defined as

$$\begin{aligned}\theta_2(r) &= r^3 b_{40} + r^2 b_{38} + r b_{39} + b_{41} \ln(r) + b_{42}, \\ \sigma_2(r) &= r^2 b_{28} + r b_{27} + b_{32} \ln(r) + b_{31}.\end{aligned}\tag{1.67}$$

Using all these solutions into Eq. (1.58), and setting $x \rightarrow 1$, we finally arrive at

$$\sigma = b_{28} r^2 + r b_{35} + b_{34} \ln r + b_{33},\tag{1.68}$$

$$\theta = b_{40} r^3 + r^2 b_{43} + b_{39} r + b_{44} \ln r + b_{45}.\tag{1.69}$$

From Eq. (1.36), and boundary condition (1.52), we come to know that $h_r = 0$ i.e the continuity of the normal component of the magnetic field across the boundary gives that induced magnetic field in the radial direction is zero. Eqs. (1.39) and (1.42) take the form

$$\frac{\partial p}{\partial z} = \frac{1}{r} \frac{\partial}{\partial r} \left(r \frac{\partial w}{\partial z} \right) + S^2 R_y \frac{\partial h_z}{\partial r} \left(\frac{r_2}{r} \right) + g_r \theta + b_r \sigma,\tag{1.70}$$

$$-R_m r_2 \frac{\partial w}{\partial r} = \frac{\partial}{\partial r} \left(r \frac{\partial h_z}{\partial r} \right).\tag{1.71}$$

Integration of Eq. (1.71) with respect to r takes the form

$$\frac{\partial h_z}{\partial r} = -\frac{R_m r_2}{r} w - \frac{c_1}{r_1},\tag{1.72}$$

where c_1 is constant.

To determine the constant c_1 , we find from Eqs. (1.3) and (1.72) that

$$J_0 = -\frac{\partial h_z}{\partial r} = \frac{R_m r_2}{r} w + \frac{c_1}{r_1},\tag{1.73}$$

since $J_0 = 0$ at $r = r_2$, so $c_1 = R_m r_2$, which gives

$$J_0 = -\frac{\partial h_z}{\partial r} = \frac{R_m r_2}{r} (w + 1). \quad (1.74)$$

Eliminating $\frac{\partial h_z}{\partial r}$ from Eqs. (1.70) and (1.74), we get

$$\frac{\partial p}{\partial z} = \frac{1}{r} \frac{\partial}{\partial r} \left(r \frac{\partial w}{\partial z} \right) - S^2 R_y \frac{R_m r_2}{r} (w + 1) \left(\frac{r_2}{r} \right) + g_r \theta + b_r \sigma, \quad (1.75)$$

i.e

$$\frac{\partial^2 w}{\partial z^2} + \frac{1}{r} \frac{\partial w}{\partial r} - M^2 \frac{r_2^2}{r^2} w = -\frac{\partial p}{\partial z} + M^2 \frac{r_2^2}{r^2} - g_r \theta - b_r \sigma, \quad (1.76)$$

where $M^2 = S^2 R_y R_m$.

The homogeneous and nonhomogeneous solutions of the above equation are defined as

$$w_c = c_2 r^B + c_3 r^{-B}, \quad (1.77)$$

$$w_p = \frac{\partial p}{\partial z} \frac{r^2}{(4 - B^2)} - 1 - g_r \left(\frac{b_{40} r^5}{25 - B^2} + \frac{b_{43} r^4}{16 - B^2} + \frac{b_{39} r^3}{9 - B^2} + \frac{b_{45} r^2}{4 - B^2} + \frac{b_{44}}{B^2} \right) - b_r \left(\frac{b_{33} r^2}{4 - B^2} + \frac{b_{35} r^3}{9 - B^2} + \frac{b_{28} r^4}{16 - B^2} + \frac{b_{34}}{B^2} \right). \quad (1.78)$$

The general solution finally takes the form

$$w = c_2 r^B + c_3 r^{-B} + \frac{\partial p}{\partial z} \frac{r^2}{(4 - B^2)} - 1 - g_r \left(\frac{b_{40} r^5}{25 - B^2} + \frac{b_{43} r^4}{16 - B^2} + \frac{b_{39} r^3}{9 - B^2} + \frac{b_{45} r^2}{4 - B^2} + \frac{b_{44}}{B^2} \right) - b_r \left(\frac{b_{33} r^2}{4 - B^2} + \frac{b_{35} r^3}{9 - B^2} + \frac{b_{28} r^4}{16 - B^2} + \frac{b_{34}}{B^2} \right), \quad (1.79)$$

where c_2 and c_3 are constants.

Using the boundary conditions, we finally arrive at

$$\begin{aligned}
w = r^B & \left(b_{46} + \frac{(r_1^{2+B} - r_2^{2+B})}{r_1^{2B} - r_2^{2B}} \frac{\partial p / \partial z}{(B^2 - 4)} \right) + r^{-B} \left(b_{47} + \frac{r_1^B r_2^B (r_1^B r_2^2 - r_1^2 r_2^B)}{r_1^{2B} - r_2^{2B}} \frac{\partial p / \partial z}{(B^2 - 4)} \right) \\
& + \frac{\partial p}{\partial z} \frac{r^2}{(4 - B^2)} - 1 - g_r \left(\frac{b_{40} r^5}{25 - B^2} + \frac{b_{43} r^4}{16 - B^2} + \frac{b_{39} r^3}{9 - B^2} + \frac{b_{45} r^2}{4 - B^2} + \frac{b_{44}}{B^2} \right) \\
& - b_r \left(\frac{b_{33} r^2}{4 - B^2} + \frac{b_{35} r^3}{9 - B^2} + \frac{b_{28} r^4}{16 - B^2} + \frac{b_{34}}{B^2} \right). \tag{1.80}
\end{aligned}$$

The axial induced magnetic field is given as

$$\begin{aligned}
h_z = -R_m r_2 & \left[\left(\frac{r^B - r_2^B}{B} \right) \left(b_{46} + \frac{(r_1^{2+B} - r_2^{2+B})}{r_1^{2B} - r_2^{2B}} \frac{\partial p / \partial z}{(B^2 - 4)} \right) - \left(b_{47} + \frac{r_1^B r_2^B (r_1^B r_2^2 - r_1^2 r_2^B)}{r_1^{2B} - r_2^{2B}} \frac{\partial p / \partial z}{(B^2 - 4)} \right) \right. \\
& \left. \left(\frac{r^{-B} - r_2^{-B}}{B} \right) + \frac{\partial p}{\partial z} \frac{(r^2 - r_2^2)}{2(4 - B^2)} - g_r \left(\frac{b_{40} (r^5 - r_2^5)}{5(25 - B^2)} + \frac{b_{43} (r^4 - r_2^4)}{4(16 - B^2)} + \frac{b_{39} (r^3 - r_2^3)}{3(9 - B^2)} \right) \right. \\
& + \frac{b_{45} (r^2 - r_2^2)}{2(4 - B^2)} + \frac{b_{44}}{B^2} (\ln r - \ln r_2) - b_r \left(\frac{b_{33} (r^2 - r_2^2)}{2(4 - B^2)} + \frac{b_{35} (r^3 - r_2^3)}{3(9 - B^2)} \right. \\
& \left. \left. + \frac{b_{28} (r^4 - r_2^4)}{4(16 - B^2)} + \frac{b_{34}}{B^2} (\ln r - \ln r_2) \right) \right]. \tag{1.81}
\end{aligned}$$

From Eqs. (1.80) and (1.81), the current density distribution become

$$\begin{aligned}
J_o = R_m r_2 & \left[r^{B-1} \left(b_{46} + \frac{(r_1^{2+B} - r_2^{2+B})}{r_1^{2B} - r_2^{2B}} \frac{\partial p / \partial z}{(B^2 - 4)} \right) + r^{-B-1} \left(b_{47} + \frac{r_1^B r_2^B (r_1^B r_2^2 - r_1^2 r_2^B)}{r_1^{2B} - r_2^{2B}} \frac{\partial p / \partial z}{(B^2 - 4)} \right) \right. \\
& + \frac{\partial p}{\partial z} \frac{r}{(4 - B^2)} - g_r \left(\frac{b_{40} r^4}{25 - B^2} + \frac{b_{43} r^3}{16 - B^2} + \frac{b_{39} r^2}{9 - B^2} + \frac{b_{45} r^1}{4 - B^2} + \frac{b_{44}}{r B^2} \right) \\
& \left. - b_r \left(\frac{b_{33} r}{4 - B^2} + \frac{b_{35} r^2}{9 - B^2} + \frac{b_{28} r^3}{16 - B^2} + \frac{b_{34}}{r B^2} \right) \right]. \tag{1.82}
\end{aligned}$$

From Eqs (1.46), (1.51) and (1.80), the pressure gradient takes the following form

$$\frac{\partial p}{\partial z} = \frac{\theta - \left(1 + \frac{\alpha^2}{2} \right) + \epsilon^2 - b_{48}}{b_{49}}. \tag{1.83}$$

The pressure rise P' and the frictional forces on the outer and inner tubes $F^{(0)}$ and $F^{(i)}$ in non-dimensional form are defined as

$$P' = \int_0^1 \frac{\partial p}{\partial z} dz, \quad (1.84)$$

$$F^{(0)} = \int_0^1 r_2^2 \left(-\frac{\partial p}{\partial z}\right) dz, \quad (1.85)$$

$$F^{(i)} = \int_0^1 r_1^2 \left(-\frac{\partial p}{\partial z}\right) dz. \quad (1.86)$$

The expression for pressure rise P' and the friction forces are considered numerically by mathematica, where as constants are defined in appendix I.

The velocities in terms of stream functions are defined as [1]

$$u = \frac{-\delta}{r} \left(\frac{\partial \Psi}{\partial z}\right) \text{ and } w = \frac{1}{r} \left(\frac{\partial \Psi}{\partial r}\right). \quad (1.87)$$

Making use of Eq. (1.80) into Eq. (1.87), we get stream function as

$$\begin{aligned} \Psi = & \left(\frac{r^{B+2} - r_1^{B+2}}{B+2} \right) \left(b_{46} + \frac{(r_1^{2+B} - r_2^{2+B})}{r_1^{2B} - r_2^{2B}} \frac{\partial p / \partial z}{(B^2 - 4)} \right) + \left(\frac{r^{-B+2} - r_1^{-B+2}}{-B+2} \right) \\ & \left(b_{47} + \frac{r_1^B r_2^B (r_1^B r_2^2 - r_1^2 r_2^B)}{r_1^{2B} - r_2^{2B}} \frac{\partial p / \partial z}{(B^2 - 4)} \right) + \left(\frac{r^4 - r_1^4}{4} \right) \frac{\partial p / \partial z}{(4 - B^2)} - \left(\frac{r^2 - r_1^2}{2} \right) \\ & - g_r \left(\frac{b_{40}}{25 - B^2} \left(\frac{r^7 - r_1^7}{7} \right) + \frac{b_{43}}{16 - B^2} \left(\frac{r^6 - r_1^6}{6} \right) + \frac{b_{39}}{9 - B^2} \left(\frac{r^5 - r_1^5}{5} \right) \right. \\ & \left. + \frac{b_{45}}{4 - B^2} \left(\frac{r^4 - r_1^4}{4} \right) + \frac{b_{44}}{B^2} \left(\frac{r^2 - r_1^2}{2} \right) \right) - b_r \left(\frac{b_{33}}{4 - B^2} \left(\frac{r^4 - r_1^4}{4} \right) \right. \\ & \left. + \frac{b_{35}}{9 - B^2} \left(\frac{r^5 - r_1^5}{5} \right) + \frac{b_{28}}{16 - B^2} \left(\frac{r^6 - r_1^6}{6} \right) + \frac{b}{B^2} \left(\frac{r^2 - r_1^2}{2} \right) \right). \quad (1.88) \end{aligned}$$

1.6 Results and discussion

1.6.1 Pumping characteristics

This subsection explains the effects of various parameters emerging in the analysis on pressure gradient $\frac{\partial p}{\partial z}$, frictional forces $F^{(0)}$ and $F^{(i)}$ and pressure rise per wavelength P' . These effects are shown in *Figs. 1.2 – 1.5*. In *Fig. 1.2*, the variation of pressure gradient versus axial coordinate z is shown for different values of M and ϵ and by fixing the remaining parameters. As M and ϵ increase, the maximum amplitude of pressure gradient increases. It can be seen that in wider part of annulus $z \in [0, 0.5]$ the pressure gradient is small and in the narrow section $z \in [0.5, 1]$ the pressure gradient is relatively large i.e. in wider portion flow can easily pass without imposition of large pressure gradient where as in narrow part a much larger pressure gradient is required to maintain the same flux to pass through it, especially at the narrowest point $z = 0.75$. This agrees with the physical situation. The variation of pressure rise P' with volume flow rate θ invested for different values of Hartmann number M and radius ratio ϵ is presented in *Fig. 1.3*. It is seen that there is inverse relation between pressure rise and flow rate i.e increase in flow rate reduces the pressure rise and thus maximum flow rate is achieved at minimum pressure rise and maximum pressure occurs at zero flow rate. Also due to increase in M and ϵ , pressure rise increases. The pumping regions, peristaltic pumping ($\theta > 0$ and $P' > 0$), augmented pumping ($\theta > 0$ and $P' < 0$) and retrograde pumping ($\theta < 0$ and $P' > 0$) are also shown in *Fig. 1.3*. It is obvious that pumping region become wider as M and ϵ increase. In *Figs. 1.4* and *1.5* friction forces for inner and outer walls versus flow rate are described. These forces possess opposite behaviour to that of pressure rise where as inner friction force behaves similar to outer friction force for the same values of parameters, moreover outer friction is larger than inner friction force for same value of various parameters.

1.6.2 Nanoparticle Phenomena

The nanoparticle phenomena σ for different values of the Brownian motion parameter N_b and the thermophoresis parameter N_t is shown in *Figs. 1.6* and *1.7*. It is seen that with increasing Brownian motion parameter N_b the concentration decreases in the region $r \in [0, 0.2]$ and increases in the region $r \in [0.2, 1]$. It can be analyzed through figures that Brownian mo-

tion parameter N_b and the thermophoresis parameter N_t have opposite effects on nanoparticle phenomena. Effects of temperature profile have also been discussed in *Figs.* 1.8 and 1.9. We observe that the temperature profile decreases in the region $r \in [0, 0.2]$ and increases in the region $r \in [0.2, 1]$ for increasing Brownian motion parameter N_b . Similar behaviour is seen for thermophoresis parameter N_t .

1.6.3 Magnetic Field Characteristics

The distribution of axial induced magnetic field h_z at line $r = 0.4$ and for other fixed set of parameters with different values of M along axial coordinates z is displayed in *Fig.*1.10. It can be seen that by increasing the Hartmann number M the axial induced magnetic field h_z also increases. In *Fig.*1.11, the effects of magnetic Reynolds number R_m on axial induced magnetic field is shown. It is observed that axial induced magnetic field h_z increases as magnetic Reynolds number increases.

The *Figs.*1.12 to 1.14 present the variation of axial induced magnetic field h_z across the annulus for several values of θ , M and R_m . By increasing the Hartmann number M , the axial induced magnetic field h_z increases. The graphical results shown in *Fig.*1.13, present that an increase in magnetic Reynolds number R_m results in an increase in the magnitude of axial induced magnetic field h_z . *Fig.*1.14 depicts the effect of mean volume flow rate θ on h_z . Clearly an increase in θ is followed by an increase in axial induced magnetic field h_z .

The variation of the current density J_o at the inlet of annulus i.e. at $z = 0$, for different values of Hartmann number M and magnetic Reynolds number R_m is observed in *Figs.*1.15 and 1.16. It is observed that for increase in both M and R_m result the increase of current density.

1.6.4 Fluid Trapping

Trapping is the phenomena in which an internal circulating bolus of the fluid by closed streamline is formed and this bolus is pulled forward along with the peristaltic wave. Effects of Hartmann number M and radius ratio ϵ are shown in *Figs.*1.17 and 1.18. In *Fig.*1.17, the effect of Hartmann number M on trapping is shown, it is seen that the volume of the bolus first increases with the increase of Hartmann number M and for $M = 1$, the bolus decreases. It is

also observed that as M increases more trapped bolus appear. Similar behaviour is observed for the variation of ϵ in Fig.1.18.

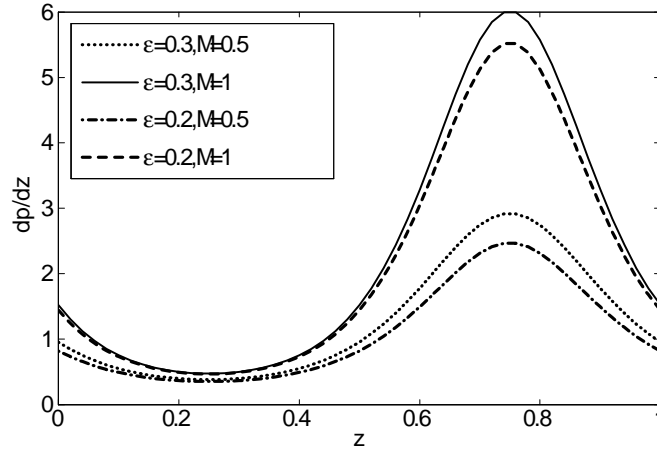


Fig. 1.2 : The variation of pressure gradient dp/dz with z for different values of M and ϵ at $\theta = -0.5$, $\alpha = 0.32$, $G_r = 0.3$, $B_r = 0.2$, $N_b = 0.3$, $N_t = 0.3$.

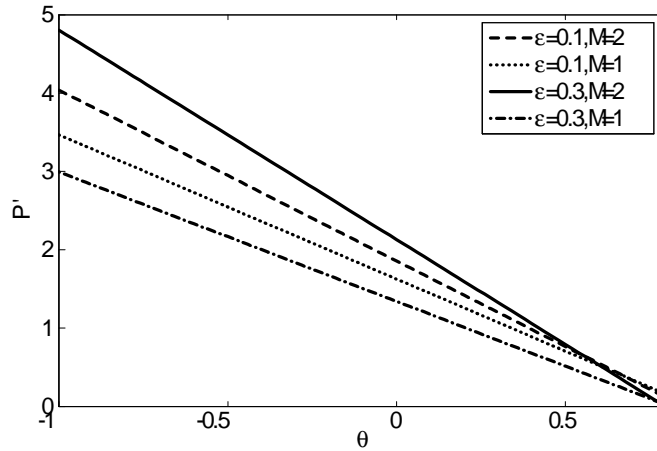


Fig. 1.3 : The variation of pressure rise P' with θ for different values of M and ϵ at $\alpha = 0.32$, $G_r = 0.3$, $B_r = 0.2$, $N_b = 0.3$, $N_t = 0.3$.

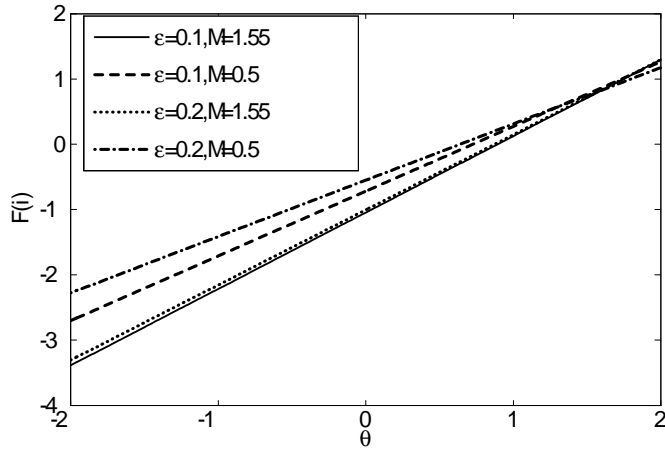


Fig. 1.4 : The variation of friction force $F(i)$ (on outer wall) with θ for different values of M and ϵ at $\alpha = 0.32$, $G_r = 0.3$, $B_r = 0.2$, $N_b = 0.3$, $N_t = 0.3$.

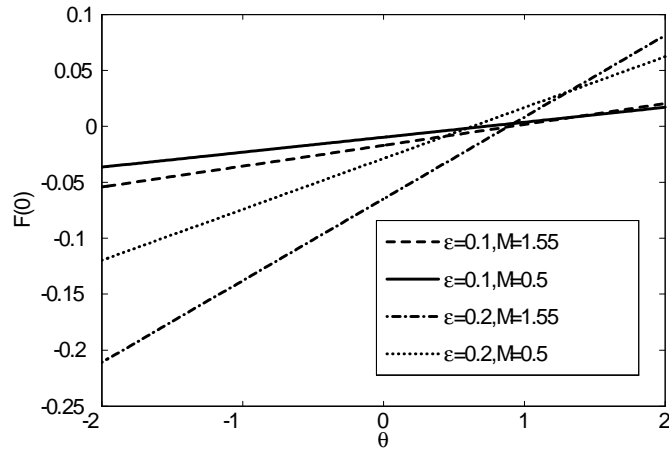


Fig. 1.5 : The variation of friction force $F(0)$ (on inner wall) with θ for different values of M and ϵ at $\alpha = 0.32$, $G_r = 0.3$, $B_r = 0.2$, $N_b = 0.3$, $N_t = 0.3$.

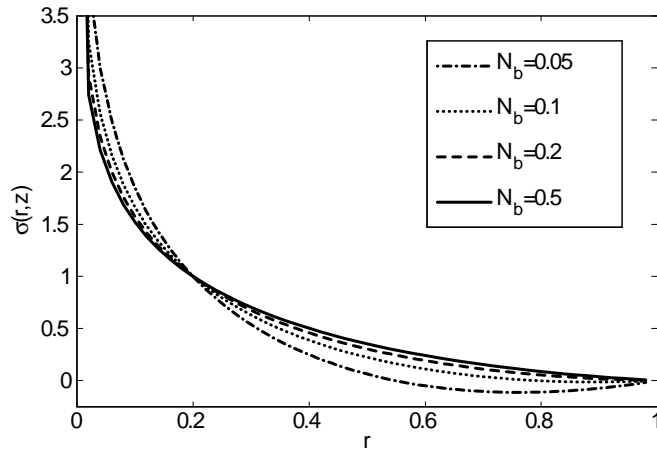


Fig. 1.6 : The variation of concentration profile with r for different values of N_b and $\alpha = 0.32$, $G_r = 0.3$, $B_r = 0.2$, $N_t = 0.3$ and $z = 0.5$.

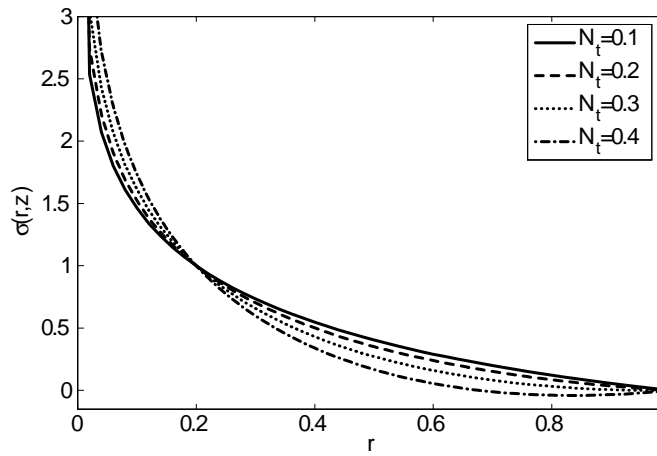


Fig. 1.7 : The variation of concentration profile with r for different values of N_t and $\alpha = 0.32$, $G_r = 0.3$, $B_r = 0.2$, $N_b = 0.3$ and $z = 0.5$.

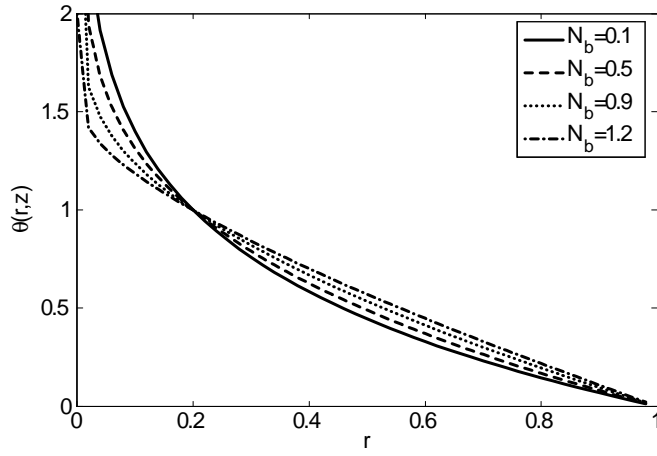


Fig. 1.8 : The variation of temperature profile with r for different values of N_b and $\alpha = 0.32$, $G_r = 0.3$, $B_r = 0.2$, $N_t = 0.3$ and $z = 0.5$.

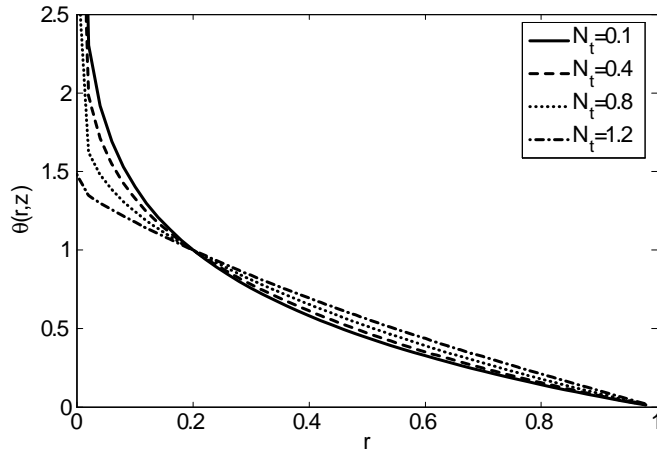


Fig. 1.9 : The variation of temperature profile with r for different values of N_t and $\alpha = 0.32$, $G_r = 0.3$, $B_r = 0.2$, $N_b = 0.3$ and $z = 0.5$.

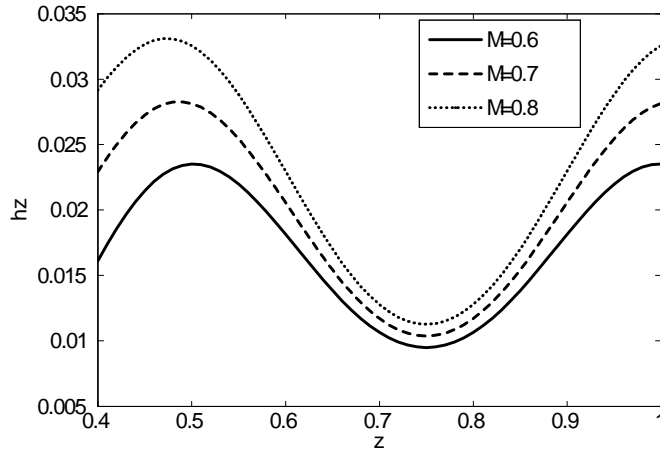


Fig. 1.10 : The variation of axial induced magnetic field h_z with the axial coordinate z for different values of M at $\theta = 2$, $\alpha = 0.2$, $\epsilon = 0.5$, $R_m = 5$, $G_r = 0.3$, $B_r = 0.2$, $N_b = 0.3$, $N_t = 0.3$ at $r = 0.4$.

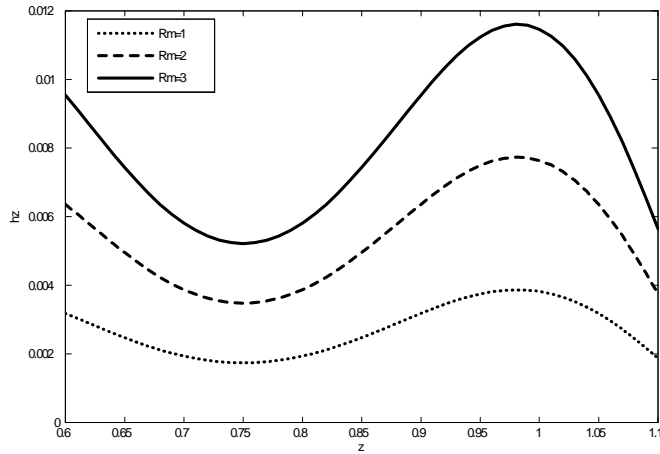


Fig. 1.11 : The variation of axial induced magnetic field h_z with the axial coordinate z for different values of R_m at $\theta = 2$, $\alpha = 0.2$, $\epsilon = 0.5$, $M = 0.5$, $G_r = 0.3$, $B_r = 0.2$, $N_b = 0.3$, $N_t = 0.3$ at $r = 0.4$.

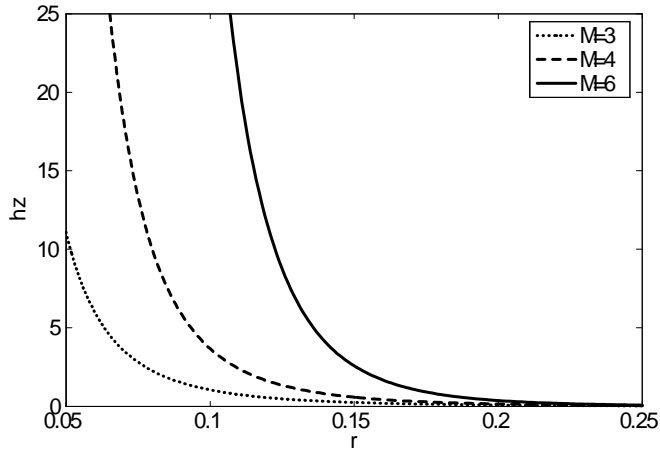


Fig. 1.12 : The variation of axial induced magnetic field h_z across the annulus for $\theta = 0.5$, $\alpha = 0.2, \epsilon = 0.05, R_m = 0.5, G_r = 0.3, B_r = 0.2, N_b = 0.3, N_t = 0.3$ and $z = 0.4$ and different values of M where $r \in [\epsilon, r_2]$.

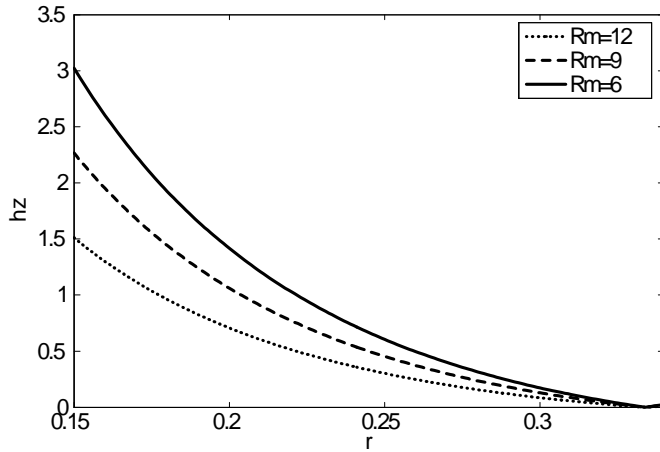


Fig. 1.13 : The variation of axial induced magnetic field h_z across the annulus for $\theta = 0.5$, $\alpha = 0.2, \epsilon = 0.05, M = 0.5, G_r = 0.3, B_r = 0.2, N_b = 0.3, N_t = 0.3$ and $z = 0.4$ and different values of M where $r \in [\epsilon, r_2]$.

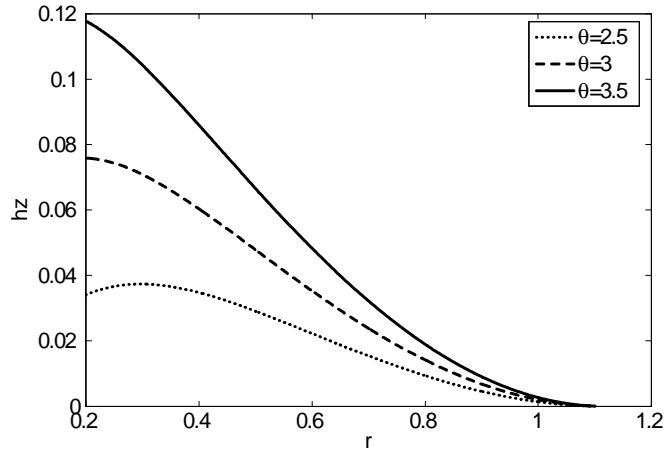


Fig. 1.14 : The variation of axial induced magnetic field h_z across the annulus for $M = 0.5$, $\alpha = 0.2$, $\epsilon = 0.1$, $R_m = 0.7$, $G_r = 0.3$, $B_r = 0.2$, $N_b = 0.3$, $N_t = 0.3$ and $z = 0.4$ and different values of M where $r \in [\epsilon, r_2]$.

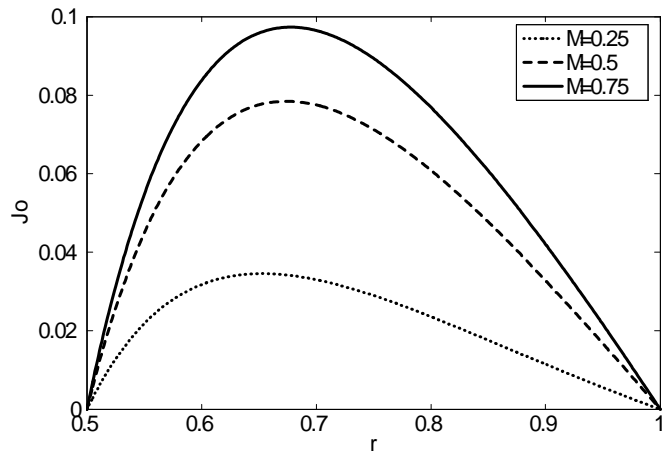


Fig. 1.15 : The variation of current density distribution J_o across the annulus for $\theta = -0.5$, $\alpha = 0.2$, $\epsilon = 0.5$, $R_m = 1$, $G_r = 0.3$, $B_r = 0.3$, $N_b = 0.3$, $N_t = 0.3$ and $z = 0$ and different values of M where $r \in [\epsilon, r_2]$.

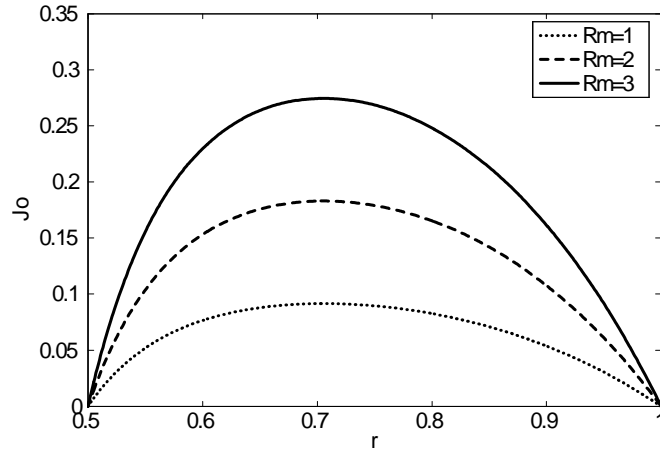
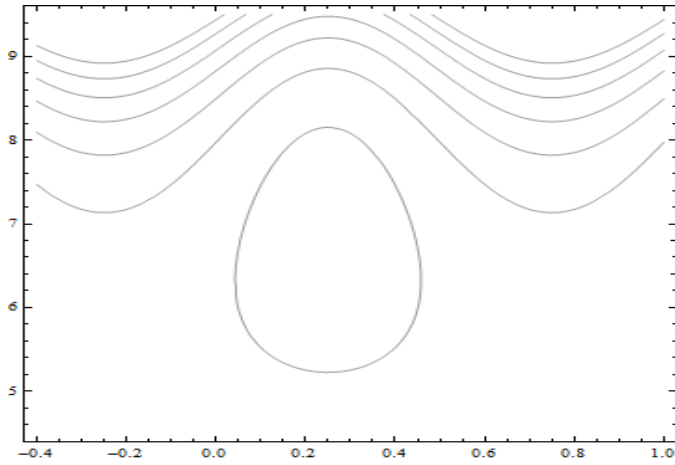
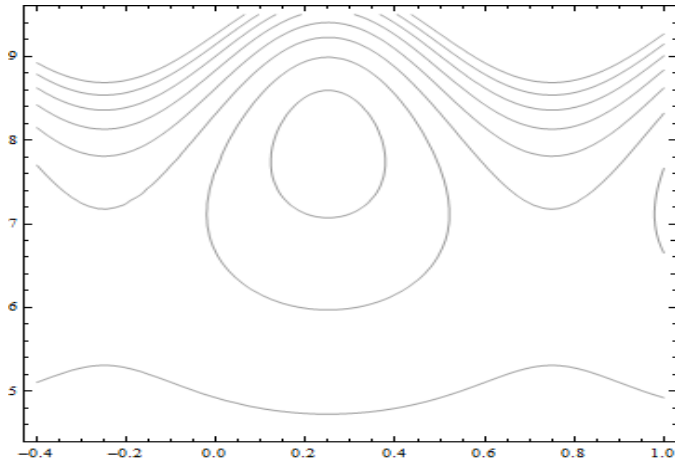


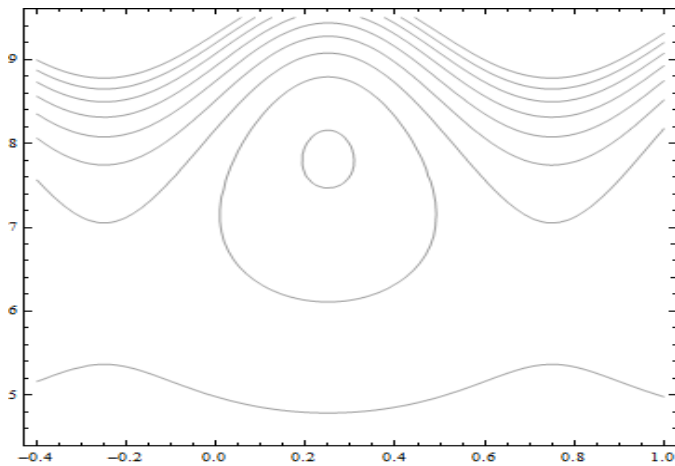
Fig. 1.16 : The variation of current density distribution J_o across the annulus for $\theta = -0.5$, $\alpha = 0.2$, $\epsilon = 0.5$, $M = 6$, $G_r = 0.3$, $B_r = 0.3$, $N_b = 0.3$, $N_t = 0.3$ and $z = 0$ and different values of $R_m = 1$ where $r \in [\epsilon, r_2]$.



(a)

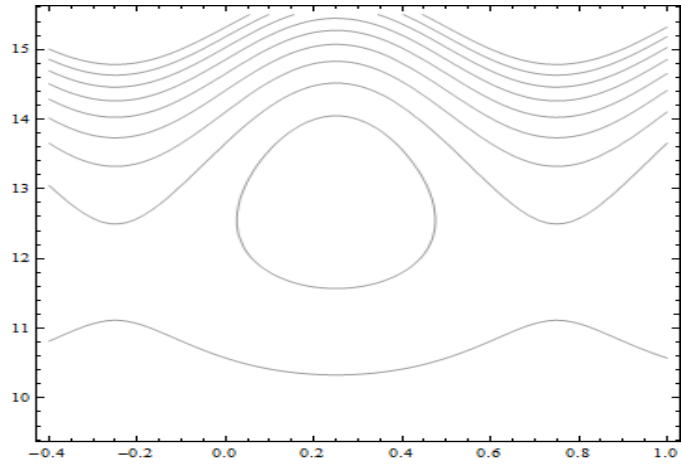


(b)

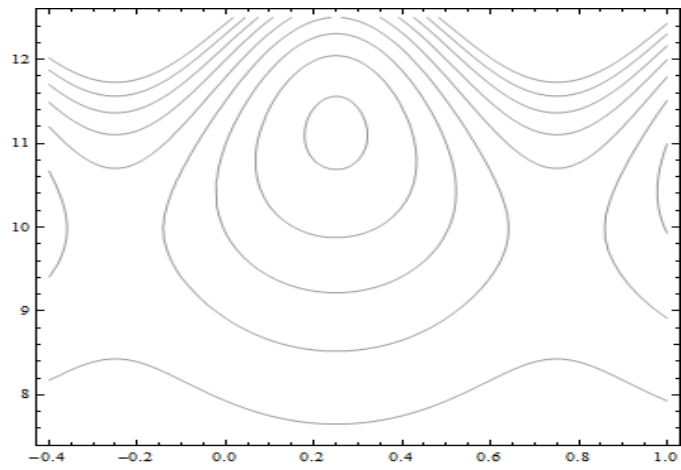


(c)

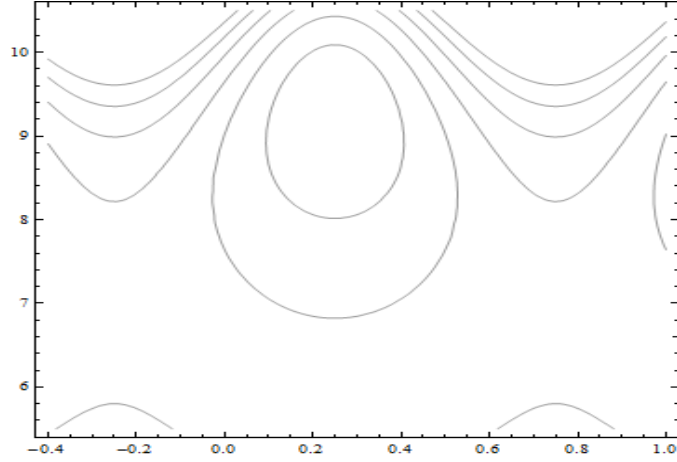
Fig. 1.17 : Plot showing streamlines for different values of Hartmann number $M = 0.5, 0.75, 1$ (a, b, c respectively) for $\alpha = 0.03, \theta = 1, \epsilon = 0.2$ and $G_r = 0.3, B_r = 0.3, N_b = 0.3, N_t = 0.3$.



(a)



(b)



(c)

Fig. 1.18 : Plot showing the streamlines for different values of radius ratio $\epsilon = 0.05, 0.1, 0.15$ (*a, b, c* respectively) for $\alpha = 0.03, \theta = 1, M = 0.5$ and $G_r = 0.3, B_r = 0.3, N_b = 0.3, N_t = 0.3$.

1.7 Concluding Remarks

Peristaltic flow of a nano fluid through an annulus is studied theoretically under the effects of the induced magnetic field. The expressions for axial pressure gradient, current density, axial magnetic field and stream functions are obtained analytically. Graphical results are shown for pressure gradient, pressure rise per wavelength, frictional forces, axial induced magnetic field, current density and trapping. The main points are summarized as

(i) As the radius ratio and Hartmann number increase, the maximum amplitude of pressure gradient increases.

(ii) With increasing flow rate the pressure rise decreases i.e. there is an inverse relation between P' and θ .

(iii) The behaviour of inner and outer frictional forces is opposite to the pressure rise.

(iv) The effects of Brownian motion parameter N_b and thermophoresis parameter N_t are

same for temperature profile.

(v) The Brownian motion parameter N_b and thermophoresis parameter N_t have opposite behaviour for concentration profile.

(vi) The axial induced magnetic field h_z increases along axial coordinates as Hartmann number and magnetic Reynolds number increase.

(vii) The axial induced magnetic field h_z increases across the annulus by increasing the Hartmann number and flow rate, and it decreases with increasing magnetic Reynolds number.

(viii) Current density and magnetic Reynolds number behave likely i.e. by increasing the magnetic Reynolds number, the current density also increases.

(ix) The volume of trapped bolus increases as Hartmann number M increases and at $M = 1$, this behaviour is reversed.

(x) By increasing the radius of the inner tube more trapped bolus are seen.

1.8 Appendix I

$$\begin{aligned}
b_1 &= r_1 - r_2, & b_2 &= \ln r_1 - \ln r_2, & b_3 &= N_b + N_t, & b_4 &= r_1^2 - r_2^2, & b_5 &= b_4 b_3, & b_6 &= 4b_1^2, \\
b_7 &= \frac{1}{b_2} + \frac{b_5}{b_2 b_6}, & b_8 &= \frac{r_2^2 b_3}{4b_1^2}, & b_9 &= b_7 \ln r, & b_{10} &= b_8 - b_9, & b_{11} &= \frac{r_2}{r_1 - r_2}, & b_{12} &= \frac{b_3}{4b_1^2}, \\
b_{13} &= b_{10} + b_{11}, & b_{14} &= \frac{b_3}{N_b b_2}, & b_{15} &= -b_{14} \ln r_2, & b_{16} &= -\frac{b_3}{N_b b_1}, & b_{17} &= \frac{b_3 b_{11}}{N_b}, & b_{18} &= \frac{N_t}{N_b}, \\
b_{19} &= b_4 b_{12}, & b_{20} &= b_7 b_2, & b_{21} &= \frac{b_{18}}{b_2}, & b_{22} &= -b_{21} - b_{21} b_{19} + b_{21} b_{20}, & b_{23} &= b_{12} r_2^2, \\
b_{24} &= b_7 \ln r_2, & b_{25} &= b_{22} \ln r_2, & b_{26} &= b_{18} (-b_{11} - b_{23} + b_{13} + b_{24} - b_{25}), & b_{27} &= \frac{b_{18}}{b_1}, \\
b_{28} &= b_{18} b_{12}, & b_{29} &= -b_{18} b_{13}, & b_{30} &= -b_{18} b_7, & b_{31} &= b_{29} + b_{26}, & b_{32} &= b_{30} + b_{22}, \\
b_{33} &= -b_{11} + b_{17} + b_{15} + b_{31}, & b_{34} &= b_{14} + b_{32}, & b_{35} &= \frac{1}{b_1} + b_{16} + b_{27}, & b_{36} &= b_{16} - \frac{1}{b_1} \\
b_{37} &= b_{14} + b_7, & b_{38} &= -\frac{N_b b_{36}}{4b_1} + \frac{N_t}{2b_1^2}, & b_{39} &= -\frac{N_b b_{37}}{b_1} - \frac{2N_t b_7}{b_1}, & b_{40} &= \frac{2N_b b_{12}}{9b_1} + \frac{4N_t b_{12}}{9b_1}, \\
b_{41} &= \frac{b_{38} (r_2^2 - r_1^2) + b_{39} (r_2 - r_1) + b_{40} (r_2^3 - r_1^3)}{\ln r_1 - \ln r_2}, \\
b_{42} &= \frac{b_{38} (r_2^2 \ln r_1 - r_1^2 \ln r_2) + b_{39} (r_2 \ln r_1 - r_1 \ln r_2) + b_{40} (r_2^3 \ln r_1 - r_1^3 \ln r_2)}{\ln r_2 - \ln r_1}, & b_{43} &= b_{38} - b_{12}, \\
b_{44} &= b_7 + b_{41}, & b_{45} &= b_{13} - b_{11} + b_{42}, \\
b_{46} &= \frac{1}{r_1^{2B} - r_2^{2B}} [g_r (b_{40} \left(\frac{r_1^{5+B} - r_2^{5+B}}{25 - B^2} \right) + b_{43} \left(\frac{r_1^{4+B} - r_2^{4+B}}{16 - B^2} \right) + b_{39} \left(\frac{r_1^{3+B} - r_2^{3+B}}{9 - B^2} \right) + \\
& b_{45} \left(\frac{r_1^{2+B} - r_2^{2+B}}{4 - B^2} \right) + b_{44} \left(\frac{r_1^B - r_2^B}{B^2} \right)) + b_r (b_{33} \left(\frac{r_1^{2+B} - r_2^{2+B}}{4 - B^2} \right) + b_{35} \left(\frac{r_1^{3+B} - r_2^{3+B}}{9 - B^2} \right) \\
& + b_{28} \left(\frac{r_1^{4+B} - r_2^{4+B}}{16 - B^2} \right) + b_{34} \left(\frac{r_1^B - r_2^B}{B^2} \right))] , \\
b_{47} &= \frac{r_1^B r_2^B}{(r_1^{2B} - r_2^{2B})} \left[g_r \left(b_{40} \left(\frac{r_1^B r_2^5 - r_1^5 r_2^B}{25 - B^2} \right) + b_{43} \left(\frac{r_1^B r_2^4 - r_1^4 r_2^B}{16 - B^2} \right) + b_{39} \left(\frac{r_1^B r_2^3 - r_1^3 r_2^B}{9 - B^2} \right) + \right. \right. \\
& b_{45} \left(\frac{r_1^B r_2^2 - r_1^2 r_2^B}{4 - B^2} \right) + b_{44} \left(\frac{r_1^B - r_2^B}{B^2} \right) \left. \right) + b_r \left(\left(b_{33} \left(\frac{r_1^B r_2^2 - r_1^2 r_2^B}{4 - B^2} \right) + b_{35} \left(\frac{r_1^B r_2^3 - r_1^3 r_2^B}{9 - B^2} \right) \right) \right. \\
& \left. \left. + b_{28} \left(\frac{r_1^B r_2^4 - r_1^4 r_2^B}{16 - B^2} \right) + b_{34} \left(\frac{r_1^B - r_2^B}{B^2} \right) \right) \right] ,
\end{aligned}$$

$$\begin{aligned}
b_{48} &= 2 \left[\frac{b_{46}}{B+2} \left(r_2^{2+B} - r_1^{2+B} \right) + \frac{b_{47}}{-B+2} \left(r_2^{2-B} - r_1^{2-B} \right) - \frac{(r_2^2 - r_1^2)}{2} - g_r \left(b_{40} \left(\frac{r_2^7 - r_1^7}{7(25 - B^2)} \right) \right) \right. \\
&\quad + b_{43} \left(\frac{r_2^6 - r_1^6}{6(16 - B^2)} \right) + b_{39} \left(\frac{r_2^5 - r_1^5}{5(9 - B^2)} \right) + b_{45} \left(\frac{r_2^4 - r_1^4}{4(4 - B^2)} \right) + b_{44} \left(\frac{r_2^2 - r_1^2}{2B^2} \right) \\
&\quad \left. - b_r \left(b_{33} \left(\frac{r_2^4 - r_1^4}{4(4 - B^2)} \right) + b_{35} \left(\frac{r_2^5 - r_1^5}{5(9 - B^2)} \right) + b_{28} \left(\frac{r_2^6 - r_1^6}{6(16 - B^2)} \right) + b_{34} \left(\frac{r_2^2 - r_1^2}{2B^2} \right) \right) \right], \\
b_{49} &= 2 \left[\frac{r_2^4 - r_1^4}{4(4 - B^2)} + \frac{r_2^{2+B} - r_1^{2+B}}{B+2} \left(\frac{r_1^{2+B} - r_2^{2+B}}{(B^2 - 4)(r_1^{2B} - r_2^{2B})} \right) + \frac{(r_2^{2-B} - r_1^{2-B})}{-B+2} \frac{(r_1^B r_2^B)(r_1^B r_2^2 - r_1^2 r_2^B)}{(B^2 - 4)(r_1^{2B} - r_2^{2B})} \right].
\end{aligned}$$

Chapter 2

Influence of induced magnetic field on peristaltic flow of hyperbolic tangent fluid in an annulus

2.1 Introduction

This chapter deals with peristaltic flow of hyperbolic tangent in an annulus. The flow is investigated in a wave frame of reference moving with velocity of the wave c . Velocity and pressure gradient have been solved analytically by using Homotopy Perturbation Method . The effects of various emerging parameters are investigated for sinusoidal wave. Streamlines have been displayed at the end of the chapter.

2.2 Basic Equations

The basic equations of continuity, momentum and magnetohydrodynamics including magnetic induction equation in the absence of displacement current and free charges are

$$\nabla \cdot \mathbf{V}' = 0 , \tag{2.1}$$

$$\rho \frac{\mathbf{D}\mathbf{V}'}{\mathbf{D}t'} = -\nabla \tilde{p}' + \nabla \cdot \tilde{\boldsymbol{\tau}}' + \mu_e (\mathbf{J}' \times \mathbf{H}'^+), \quad (2.2)$$

$$\nabla \cdot \mathbf{H}'^+ = 0, \quad (2.3)$$

$$\nabla \cdot \mathbf{E}' = 0, \quad (2.4)$$

$$\nabla \times \mathbf{H}'^+ = \mathbf{J}' \quad \text{with } \mathbf{J}' = \sigma \{ \mathbf{E}' + \mu_e (\mathbf{V}' \times \mathbf{H}'^+) \}, \quad (2.5)$$

$$\nabla \times \mathbf{E}' = -\mu_e \frac{\partial \mathbf{H}'^+}{\partial t'}, \quad (2.6)$$

$$\frac{\partial \mathbf{H}'^+}{\partial t'} = \nabla \times \{ \mathbf{V}' \times \mathbf{H}'^+ \} + \zeta \nabla^2 \mathbf{H}'^+, \quad (2.7)$$

where \mathbf{V}' is the velocity vector, \mathbf{J}' is the electric current density, \mathbf{E}' is an induced electric field, μ_e is the magnetic permeability while σ is the electrical conductivity and $\mathbf{D}/\mathbf{D}t'$ denotes material derivative, magnetic diffusivity is given as $\zeta = 1/\sigma\mu_e$ and $\tilde{\boldsymbol{\tau}}'$ is the stress tensor. The stress tensor is given as

$$\tilde{\boldsymbol{\tau}} = [\eta_\infty + (\eta_0 + \eta_\infty) \tanh(\Gamma \tilde{\boldsymbol{\gamma}})^n] \tilde{\boldsymbol{\gamma}}_i, \quad (2.8)$$

in which η_0 , η_∞ , m , Γ , denotes the zero shear rate viscosity, infinite rate of shear viscosity, power law index, and time constant respectively and $\tilde{\boldsymbol{\gamma}}$ now defined as

$$\tilde{\boldsymbol{\gamma}} = \sqrt{\frac{1}{2} \sum_i \sum_j \bar{\gamma}_{ij} \bar{\gamma}_{ji}} = \sqrt{\frac{1}{2} \boldsymbol{\pi}}, \quad (2.9)$$

where

$$\boldsymbol{\pi} = \text{trace}(\text{grad } \mathbf{V}' + (\text{grad } \mathbf{V}')^T)^2, \quad (2.10)$$

in which π is the second invariant strain tensor. We study Eq. (2.8) in the case for $\eta_\infty = 0$

and $\Gamma\tilde{\gamma} < 1$. The element of extra stress tensor so inscribed as

$$\tilde{\tau} = \eta_0[(\Gamma\tilde{\gamma})^n]\tilde{\gamma}_i = \eta_0[(1 + \Gamma\tilde{\gamma} - 1)^n]\tilde{\gamma}_i = \eta_0[1 + n(\Gamma\tilde{\gamma} - 1)]\tilde{\gamma}_i, \quad (2.11)$$

$$\tilde{\gamma}_i = \mathbf{L} + \mathbf{L}^T. \quad (2.12)$$

2.3 Formulation of the Problem

Consider unsteady flow of incompressible and electrically conducting hyperbolic tangent fluid through the gap between two coaxial tubes. Inner tube is uniform and rigid while outer tube has a sinusoidal wave travelling down its walls. We choose cylindrical coordinates (R', Z') such that R' is the radial coordinates and Z' is the axial coordinate. An external uniform magnetic field of strength $\frac{H_0 R'_2}{R'}$ is applied radially which will give rise to an induced magnetic field $\mathbf{H}'(h'_{R'}(R', Z', t'), 0, h'_{z'}(R', Z', t'))$ and total magnetic field will be $\mathbf{H}' + \left(\frac{H_0 R'_2}{R'}, 0, h'_{Z'}\right)$.

The geometrical shape is already defined in previous chapter however for the sake of easiness we define it again in *Fig.* (2.1)

$$R'_1 = a_1, \quad (2.13)$$

$$R'_2 = a_2 + b \sin \frac{2\pi}{\lambda} (Z' - ct'), \quad (2.14)$$

where a_1, a_2 are the radii of the inner and outer tubes, b is the amplitude of the wave, λ is the wavelength, c is the propagation velocity and t' is the time.

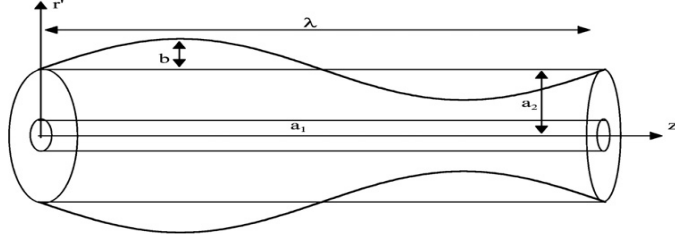


Fig.(1.2): Geometry of the problem

Eqs. (2.1) to (2.12) in component form for an incompressible tangent hyperbolic fluid with induced magnetic field take the following form

$$\frac{\partial h'_R}{\partial R'} + \frac{h'_{R'}}{R'} + \frac{\partial h'_{Z'}}{\partial Z'} = 0, \quad (2.15)$$

$$\frac{\partial \tilde{U}'}{\partial R'} + \frac{\tilde{U}'}{R'} + \frac{\partial \tilde{W}'}{\partial Z'} = 0, \quad (2.16)$$

$$\begin{aligned} \rho \left(\frac{\partial \tilde{U}'}{\partial t'} + \tilde{U}' \frac{\partial \tilde{U}'}{\partial R'} + \tilde{W}' \frac{\partial \tilde{U}'}{\partial Z'} \right) = & -\frac{\partial \tilde{p}'}{\partial R'} + \frac{1}{R'} \frac{\partial (R \tilde{\tau}_{RR})}{\partial R'} + \frac{\partial (\tilde{\tau}_{RZ})}{\partial Z'} - \frac{\tilde{\tau}_{\theta\theta}}{R'} \\ & + \mu_e h'_{Z'} \left[\frac{\partial}{\partial Z'} \left(H'_o \frac{R'_2}{R'} + h'_R \right) - \frac{\partial h'_{Z'}}{\partial R'} \right], \end{aligned} \quad (2.17)$$

$$\begin{aligned}
\rho \left(\frac{\partial \tilde{U}'}{\partial t'} + \tilde{U}' \frac{\partial \tilde{W}'}{\partial R'} + \tilde{W}' \frac{\partial \tilde{W}'}{\partial Z'} \right) &= -\frac{\partial \tilde{p}'}{\partial Z'} + \frac{1}{R'} \frac{\partial (R' \tilde{\tau}_{RZ})}{\partial R'} + \frac{\partial (\tilde{\tau}_{ZZ})}{\partial Z'} \\
+ \mu_e \left[\frac{\partial h'_Z}{\partial R'} - \frac{\partial}{\partial Z'} \left(H'_o \frac{R'_2}{R'} + h'_{R'} \right) \right] &\left(H'_o \frac{R'_2}{R'} + h'_{R'} \right), \tag{2.18}
\end{aligned}$$

$$\begin{aligned}
\left[\frac{\partial}{\partial t'} + \left(\tilde{U}' \frac{\partial}{\partial R'} + \tilde{W}' \frac{\partial}{\partial Z'} \right) - \frac{\partial \tilde{U}'}{\partial R'} \right] &\left(H'_o \frac{R'_2}{R'} + h'_{R'} \right) - \frac{\partial \tilde{U}'}{\partial R'} h'_Z \\
= \zeta \frac{\partial}{\partial Z'} \left(\frac{\partial}{\partial Z'} \left(H'_o \frac{R'_2}{R'} + h'_{R'} \right) \right) &- \left(\frac{\partial h'_Z}{\partial R'} \right), \tag{2.19}
\end{aligned}$$

$$\begin{aligned}
\left[\frac{\partial}{\partial t'} + \left(\tilde{U}' \frac{\partial}{\partial R'} + \tilde{W}' \frac{\partial}{\partial Z'} \right) - \frac{\partial \tilde{W}'}{\partial Z'} \right] &h'_z - \frac{\partial \tilde{W}'}{\partial R'} \left(H'_o \frac{R'_2}{R'} + h'_{R'} \right) \\
= \zeta \left[\frac{1}{R'} \frac{\partial}{\partial R'} \left(R' \frac{\partial h'_Z}{\partial R'} \right) - \frac{\partial}{\partial Z'} \left(\frac{\partial}{\partial R'} + \frac{1}{R'} \right) \right] &\left(H'_o \frac{R'_2}{R'} + h'_{R'} \right). \tag{2.20}
\end{aligned}$$

In the fixed coordinates (R', Z') the flow among cylinders is unsteady. It converts steady in a wave structure (r', z') moving with similar speed as the wave movements in the Z' direction. Both structures are connected through the following transformations.

$$r' = R', \quad z' = Z' - ct', \quad \tilde{U}' = u', \quad \tilde{W}' = w' - ct', \tag{2.21}$$

where u', w' are the velocity components in the wave structure. Suitable boundary limits in wave structures stand

$$w' = -c, \quad \text{at } r' = r'_1, \quad w' = -c, \quad \text{at } r' = r'_2 = a_2 + b \sin \frac{2\pi}{\lambda} (z'). \tag{2.22}$$

Introducing the dimensionless parameters

$$\begin{aligned}
R &= \frac{R'}{a_2}, \quad r = \frac{r'}{a_2}, \quad Z = \frac{Z'}{\lambda}, \quad z = \frac{z'}{\lambda}, \quad W = \frac{\widetilde{W}'}{c}, \quad w = \frac{w'}{c}, \quad U = \frac{\lambda \widetilde{U}'}{a_2 c}, \quad u = \frac{\lambda u'}{a_2 c}, \\
p &= \frac{a_2^2 p'}{c \lambda \mu}, \quad t = \frac{ct'}{\lambda}, \quad \hat{\delta} = \frac{a_2}{\lambda}, \quad R_y = \frac{\rho c a_2}{\mu}, \quad W_e = \frac{\Gamma c}{a_2}, \\
r_1 &= \frac{r'_1}{a_2} = \epsilon, \quad r_2 = \frac{r'_2}{H_2} = 1 + \alpha \sin 2\pi z, \quad \epsilon = \frac{a_1}{a_2}, \quad h_r = \frac{h'_{r'}}{H_0}, \quad h'_z = \frac{h_z}{H_0}.
\end{aligned} \tag{2.23}$$

We define W_e , R_y , $\hat{\delta}$, α , ϵ are the Weissenberg number, Reynolds number, wave number, α is the amplitude ratio and ϵ is radius ratio respectively.

Using Eq.(2.23), the non-dimensional form of Eqs. (2.15) to (2.20) take the form

$$\frac{\partial h_r}{\partial r} + \frac{h_r}{r} + \hat{\delta} \frac{\partial h_z}{\partial z} = 0, \tag{2.24}$$

$$\frac{\partial u}{\partial r} + \frac{u}{r} + \frac{\partial w}{\partial z} = 0, \tag{2.25}$$

$$\hat{\delta}^3 R_y \left(u \frac{\partial u}{\partial r} + w \frac{\partial u}{\partial z} \right) = -\frac{\partial p}{\partial r} + \hat{\delta}^2 \frac{\partial}{\partial z} (\tau_{rz}) + \frac{\hat{\delta}}{r} \frac{\partial}{\partial r} (r \tau_{rr}) - \frac{\hat{\delta}}{r} \tau_{\theta\theta} + S^2 R_y \left[\hat{\delta} \left(\frac{1}{r} \frac{\partial r_2}{\partial z} + \frac{\partial h_r}{\partial r} \right) - \frac{\partial h_z}{\partial r} \right] h_z, \tag{2.26}$$

$$\hat{\delta} R_y \left(u \frac{\partial w}{\partial r} + w \frac{\partial w}{\partial z} \right) = -\frac{\partial p}{\partial z} + \frac{1}{r} \frac{\partial}{\partial r} (r \tau_{rz}) + \hat{\delta} \frac{\partial}{\partial z} (\tau_{zz}) + S^2 R_y \left[\frac{\partial h_z}{\partial r} - \hat{\delta} \left(\frac{1}{r} \frac{\partial r_2}{\partial z} + \frac{\partial h_r}{\partial r} \right) \right] \left(\frac{r_2}{r} + h_r \right), \tag{2.27}$$

where

$$\begin{aligned}
\tau_{rr} &= 2\hat{\delta} [1 + n(W_e \dot{\gamma} - 1)] \frac{\partial u}{\partial r}, \\
\tau_{rz} &= [1 + n(W_e \dot{\gamma} - 1)] \left(\frac{\partial u}{\partial z} \hat{\delta}^2 + \frac{\partial w}{\partial r} \right),
\end{aligned}$$

$$\begin{aligned}
\tau_{zz} &= 2\hat{\delta}[1 + n(W_e\dot{\gamma} - 1)]\frac{\partial w}{\partial z}, \\
\tau_{\theta\theta} &= 2\hat{\delta}[1 + n(W_e\dot{\gamma} - 1)]\frac{u}{r},
\end{aligned} \tag{2.28}$$

$$\dot{\gamma} = [2\hat{\delta}^2\left(\frac{\partial u}{\partial r}\right)^2 + \left(\frac{\partial u}{\partial z}\hat{\delta}^2 + \frac{\partial w}{\partial r}\right)^2 + 2\hat{\delta}^2\left(\frac{\partial w}{\partial z}\right)^2 + 2\hat{\delta}^2\frac{u^2}{r^2}]^{\frac{1}{2}}. \tag{2.29}$$

$$\hat{\delta} \left[\frac{\partial}{\partial t} + \left(u\frac{\partial}{\partial r} + w\frac{\partial}{\partial z}\right) - \frac{\partial u}{\partial r} \right] \left(\frac{r_2}{r} + h_r\right) - \hat{\delta} \frac{\partial u}{\partial r} h_z = \frac{\hat{\delta}}{R_m} \frac{\partial}{\partial z} \left[\hat{\delta} \left(\frac{1}{r} \frac{\partial r_2}{\partial z} + \frac{\partial h_r}{\partial z} \right) - \frac{\partial h_z}{\partial r} \right], \tag{2.30}$$

$$\hat{\delta} \left[\frac{\partial}{\partial t} + \left(u\frac{\partial}{\partial r} + w\frac{\partial}{\partial z}\right) - \frac{\partial w}{\partial z} \right] h_z - \frac{\partial w}{\partial r} \left(\frac{r_2}{r} + h_r\right) = \frac{1}{R_m} \left[\frac{1}{r} \frac{\partial}{\partial r} \left(r \frac{\partial h_z}{\partial r} \right) - \hat{\delta} \frac{\partial}{\partial z} \left(\frac{\partial}{\partial r} + \frac{1}{r} \right) \left(\frac{r_2}{r} + h_r\right) \right]. \tag{2.31}$$

Under the assumption of long wavelength and dropping terms of order $\hat{\delta}$ and higher, Eqs. (2.24) to (2.31) take the form

$$\frac{\partial h_r}{\partial r} + \frac{hr}{r} = 0, \tag{2.32}$$

$$\frac{\partial u}{\partial r} + \frac{u}{r} + \frac{\partial w}{\partial z} = 0, \tag{2.33}$$

$$\frac{\partial p}{\partial r} = 0. \tag{2.34}$$

$$\frac{\partial p}{\partial z} = \frac{1}{r} \frac{\partial}{\partial r} \left(r \left(1 + n \left(W_e \frac{\partial w}{\partial z} - 1 \right) \right) \frac{\partial w}{\partial r} \right) + S^2 R_y \frac{\partial h_z}{\partial r} \left(\frac{r_2}{r} + h_r \right), \tag{2.35}$$

$$\frac{\partial w}{\partial r} \left(\frac{r_2}{r} + h_r \right) = -\frac{1}{R_m} \left[\frac{1}{r} \frac{\partial}{\partial r} \left(r \frac{\partial h_z}{\partial r} \right) \right], \tag{2.36}$$

where $S^2 = \frac{H_o^2 \mu_e}{\rho c^2}$ and $R_m = \frac{a_2}{\zeta}$ are Strommer's number (magnetic force number) and the

magnetic Reynolds number respectively. Eq. (2.34) displays that p is not a function of r .

2.4 Rate of volume flow and boundary conditions

In the fixed coordinates volume flow rate in the instantaneous position is specified by

$$\bar{Q} = 2\pi \int_{R'_1}^{R'_2} R' \widetilde{W} dR', \quad (2.37)$$

where R'_2 is a function of Z' and t' . Invoking Eq. (2.21) into Eq. (2.37) and then integrating, we obtain

$$\bar{Q} = \bar{q} + \pi c(r_2'^2 - r_1'^2), \quad (2.38)$$

where

$$\bar{q} = 2\pi \int_{r'_1}^{r'_2} r' w' dr'. \quad (2.39)$$

In the moving coordinates system the volume flow rate is independent of time as mention in Eq. (2.39). Here r'_2 is the function of z' alone. Using dimensionless variables ,we find

$$F = \frac{\bar{q}}{\pi a_2^2 c} = 2 \int_{r'_1}^{r'_2} r w dr. \quad (2.40)$$

Over a period $T = \frac{\lambda}{c}$ the time-mean flow at a fixed z position is defined as

$$\theta' = \frac{1}{T} \int_0^T \bar{Q} dt'. \quad (2.41)$$

Invoking Eq. (2.38) into Eq. (2.41) and integrating, we get

$$\theta' = \bar{q} + \pi c \left(a_2^2 - a_1^2 + \frac{b^2}{2} \right), \quad (2.42)$$

which can be inscribed as

$$\frac{\theta'}{\pi a_2^2 c} = \frac{\tilde{q}}{\pi a_2^2 c} + 1 + \frac{\alpha^2}{2} - \epsilon^2. \quad (2.43)$$

Dimensionless time-mean flow can be defined as

$$\theta = \frac{\theta'}{2\pi H_2^2 \tilde{s}}. \quad (2.44)$$

With the aid of Eq. (2.40) and (2.44), Eq. (2.43) take the form

$$\theta = F + 1 + \frac{\alpha^2}{2} - \epsilon^2. \quad (2.45)$$

The consistent dimensionless boundary conditions for the problem are defined as

$$\begin{aligned} w &= -1 \text{ at } r = r_1 = \epsilon, \quad w = -1 \text{ at } r = r_2 = 1 + \alpha \sin(2\pi z). \\ h_r &= 0, h_z = 0 \text{ at } r = r_1. \end{aligned} \quad (2.46)$$

2.5 Solution of the Problem

From Eq. (2.32), and boundary condition (2.46) we come to know that $h_r = 0$ i.e the continuity of the normal component of the magnetic field across the boundary gives that induced magnetic field in the radial direction is zero. Eq (2.35) and (2.36) become

$$\frac{\partial p}{\partial z} = \frac{1}{r} \frac{\partial}{\partial r} \left(r \left(1 + n \left(W_e \frac{\partial w}{\partial z} - 1 \right) \right) \frac{\partial w}{\partial r} \right) + S^2 R_y \frac{\partial h_z}{\partial r} \left(\frac{r_2}{r} \right), \quad (2.47)$$

$$-R_m r_2 \frac{\partial w}{\partial r} = \frac{\partial}{\partial r} \left(r \frac{\partial h_z}{\partial r} \right). \quad (2.48)$$

Simplification of Eq. (2.48) takes the form

$$\frac{\partial h_z}{\partial r} = -\frac{R_m r_2}{r} w - \frac{c_6}{r_1}, \quad (2.49)$$

where c_6 is constant.

The value of constant c_6 can be determined with the help of Eqs. (2.5) and (2.49) as

$$J_0 = -\frac{\partial h_z}{\partial r} = \frac{R_m r_2}{r} w + \frac{c_6}{r_1}, \quad (2.50)$$

since $J_0 = 0$ at $r = r_2$, so $c = R_m r_2$, which gives

$$J_0 = -\frac{\partial h_z}{\partial r} = \frac{R_m r_2}{r} (w + 1). \quad (2.51)$$

Elimination of $\frac{\partial h_z}{\partial r}$ from Eqs. (2.47) and (2.51), yields

$$2nW_e \left(\frac{\partial w}{\partial r} \right) \left(\frac{\partial^2 w}{\partial z^2} \right) + \frac{1}{r} (1-n) \frac{\partial}{\partial r} \left(r \frac{\partial w}{\partial r} \right) + \frac{1}{r} n W_e \left(\frac{\partial w}{\partial r} \right)^2 - \frac{M^2 r_2^2}{r^2} w = \frac{\partial p}{\partial z} + \frac{M^2 r_2^2}{r^2}. \quad (2.52)$$

where $M^2 = S^2 R_y R_m$.

2.5.1 Homotopy Perturbation Solution

To achieve the solution of above equation, we used homotopy perturbation method. The homotopy perturbation method advises that we write Eq. (2.52) as [15]

$$\begin{aligned} H(w, x) = & (1-x) [\mathcal{L}(w) - \mathcal{L}(w_{20})] + j \left[\mathcal{L}(w) - \frac{\partial p}{\partial z} - \frac{M^2 r_2^2}{r^2} + \frac{1}{r} n W_e \left(\frac{\partial w}{\partial r} \right)^2 \right. \\ & \left. + 2n W_e \left(\frac{\partial w}{\partial r} \right) \left(\frac{\partial^2 w}{\partial z^2} \right) \right]. \end{aligned} \quad (2.53)$$

The linear operator and the initial guesses are chosen as

$$\begin{aligned} \mathcal{L} &= \frac{1}{r} \frac{\partial}{\partial r} \left(r (1-n) \frac{\partial}{\partial r} \right) - \frac{M^2 r_2^2}{r^2}, \\ w_{20}(r, z) &= \frac{\partial p'_0}{\partial z} \left(a_4 r^k + a_5 r^{-k} + a_2 r^2 \right) - 1. \end{aligned} \quad (2.54)$$

According to HPM, we define

$$\begin{aligned} w &= w_0 + xw_1 + x^2w_2 + \dots, \\ p &= p_0 + xp_1 + x^2p_2 + \dots, \end{aligned} \quad (2.55)$$

with the help of above equations, Eq. (2.53) after equating the like powers of x give the following systems.

Zeroth-order problem

$$\begin{aligned} \mathcal{L}(w_0) - \mathcal{L}(w_{20}) &= 0, \\ w_0 &= -1 \text{ at } r = r_1, \end{aligned} \quad (2.56)$$

$$w_0 = -1 \text{ at } r = r_2. \quad (2.57)$$

First-order problem

$$\mathcal{L}(w_1) = -\mathcal{L}(w_{20}) - \frac{1}{r}nW_e \left[\frac{\partial w_o}{\partial r} \right]^2 + \frac{\partial p_1}{\partial z} + \frac{M^2 r_2^2}{r^2} - 2nW_e \frac{\partial w_o}{\partial r} \frac{\partial^2 w_o}{\partial r^2}, \quad (2.58)$$

$$w_1 = 0 \text{ at } r = r_1,$$

$$w_1 = 0 \text{ at } r = r_2 = 1 + \alpha \sin 2\pi z. \quad (2.59)$$

We can write the solutions of these problems as

Zeroth-order solution

The zeroth order solution is defined as

$$w_0(r, z) = \frac{\partial p_0}{\partial z} \left(b_4 r^k + b_5 r^{-k} + b_2 r^2 \right) - 1. \quad (2.60)$$

First-order solution

With the help of expression (2.60), solution of first order system (2.58) subject to boundary condition (2.59) is directly defined as

$$w_1(r, z) = \frac{\partial p_1}{\partial z} \left(b_4 r^k + b_5 r^{-k} + b_2 r^2 \right) + b_{54} r^k + b_{55} r^{-k} + b_{43} r^2 + b_{44} r^{2k-1} + b_{45} r^{-(2k+1)} + b_{46} r^3 + b_{47} r^{-1} + b_{48} r^{k+1} + b_{49} r^{-k+1}. \quad (2.61)$$

Using all these solutions into Eq. (2.55), and setting $x \rightarrow 1$, we finally arrive at

$$w = \frac{\partial p}{\partial z} \left(b_4 r^k + b_5 r^{-k} + b_2 r^2 \right) + b_{54} r^k + b_{55} r^{-k} + b_{43} r^2 + b_{44} r^{2k-1} + b_{45} r^{-(2k+1)} + b_{46} r^3 + b_{47} r^{-1} + b_{48} r^{k+1} + b_{49} r^{-k+1} - 1. \quad (2.62)$$

and pressure gradient takes the following form

$$\frac{\partial p}{\partial z} = b_{58} \left[\theta - \left(1 + \frac{\alpha^2}{2} \right) + \epsilon^2 \right] + b_{59}. \quad (2.63)$$

The axial induced magnetic field is given as

$$h_z = -R_m r_2 \left[\frac{\partial p}{\partial z} \left(b_4 \left(\frac{r_2^k - r^k}{k} \right) - b_5 \left(\frac{r_2^{-k} - r^{-k}}{k} \right) + b_2 \left(\frac{r_2^2 - r^2}{2} \right) \right) + b_{54} \left(\frac{r_2^k - r^k}{k} \right) - b_{55} \left(\frac{r_2^{-k} - r^{-k}}{k} \right) + b_{43} \left(\frac{r_2^2 - r^2}{2} \right) + b_{44} \left(\frac{r_2^{2k-1} - r^{2k-1}}{2k-1} \right) - b_{45} \left(\frac{r_2^{-(2k+1)} - r^{-(2k+1)}}{2k+1} \right) + b_{46} \left(\frac{r_2^3 - r^3}{3} \right) - b_{47} \left(\frac{r_2^{-1} - r^{-1}}{1} \right) + b_{48} \left(\frac{r_2^{k+1} - r^{k+1}}{k+1} \right) + b_{49} \left(\frac{r_2^{-k+1} - r^{-k+1}}{-k+1} \right) \right]. \quad (2.64)$$

From Eqs. (2.62) and (2.64), the current density distribution take the form

$$J_o = R_m r_2 \left[\frac{\partial p}{\partial z} \left(b_4 r^{k-1} + b_5 r^{-k-1} + b_2 r \right) + b_{54} r^{k-1} + b_{55} r^{-k-1} + b_{43} r + b_{44} r^{2k-2} + b_{45} r^{-(2k+2)} + b_{46} r^2 + b_{47} r^{-2} + b_{48} r^k + b_{49} r^{-k} \right]. \quad (2.65)$$

The pressure rise P' and the frictional forces the outer and inner tubes are $F(0)$ and $F(i)$ in non-dimensional forms are given by

$$P' = \int_0^1 \frac{\partial p}{\partial z} dz, \quad (2.66)$$

$$F(0) = \int_0^1 r_2^2 \left(-\frac{\partial p}{\partial z} \right) dz, \quad (2.67)$$

$$F(i) = \int_0^1 r_1^2 \left(-\frac{\partial p}{\partial z} \right) dz. \quad (2.68)$$

The expression for pressure rise P' and the friction forces are computed numerically by using mathematica, where as constants are defined in appendix.

The velocities in terms of stream functions are defined as [1]

$$u = \frac{-\delta}{r} \left(\frac{\partial \Psi}{\partial z} \right) \text{ and } w = \frac{1}{r} \left(\frac{\partial \Psi}{\partial r} \right), \quad (2.69)$$

Making use of Eq. (2.62) into Eq. (2.69), we get stream function as

$$\begin{aligned} \Psi = & \frac{\partial p}{\partial z} \left(b_4 \left(\frac{r^{k+2} - r_1^k}{k+2} \right) + b_5 \left(\frac{r^{-k+2} - r_1^{-k+2}}{-k+2} \right) + b_2 \left(\frac{r^4 - r_1^4}{4} \right) \right) \\ & + b_{54} \left(\frac{r^{k+2} - r_1^{k+2}}{k+2} \right) + b_{55} \left(\frac{r^{-k+2} - r_1^{-k+2}}{-k+2} \right) + b_{43} \left(\frac{r^4 - r_1^4}{4} \right) \end{aligned} \quad (2.70)$$

$$\begin{aligned}
& +b_{44} \left(\frac{r^{2k+1} - r_1^{2k+1}}{2k+1} \right) + b_{45} \left(\frac{r_2^{-2k+1} - r^{-2k+1}}{-2k+1} \right) + b_{46} \left(\frac{r^5 - r_1^5}{5} \right) \\
& +b_{47} \left(\frac{r - r_1}{1} \right) + b_{48} \left(\frac{r^{k+3} - r_1^{k+3}}{k+3} \right) + b_{49} \left(\frac{r_2^{-k+3} - r^{-k+3}}{-k+3} \right) \\
& - \left(\frac{r^2 - r_1^2}{2} \right)]. \tag{2.71}
\end{aligned}$$

2.6 Results and Discussion

2.6.1 Pumping Characteristics

This subsection explains the effects of various parameters emerging in the analysis on pressure gradient $\frac{\partial p}{\partial z}$, frictional forces $F(0)$ and $F(i)$ and pressure rise per wavelength P' . These effects are shown in *Figs. 2.2 – 2.13*. In *Fig. 2.2*, the variation of pressure gradient versus axial coordinate z is shown for different values of radius ratio ϵ by fixing the remaining parameters. As ϵ increase, the maximum amplitude of pressure gradient increases. The effect of Hartmann number M by taking various values is depicted in *Fig. 2.4* and it shows that by increasing M pressure gradient decreases. *Fig. 2.5* describes that by raising the value of Weissenberg number W_e , pressure gradient also elevates. It can be seen that in wider part of annulus $z \in [0, 0.5]$ the pressure gradient is small and in the narrow section $z \in [0.5, 1]$ the pressure gradient is relatively large i.e. in wider portion, flow can easily pass without imposition of large pressure gradient where as in narrow part a much larger pressure gradient is required to maintain the same flux to pass through it, especially at the narrowest point $z = 0.75$. This agrees with the physical situation. The variation of pressure rise P' with volume flow rate θ invested for different values of Hartmann number M , radius ratio ϵ and Weissenberg number W_e is presented in *Figs. 2.5 – 2.7*. It can be seen that there is inverse relation between Pressure rise and flow rate i.e. increase in flow rate reduces the pressure rise and thus maximum flow rate is achieved at minimum pressure rise and maximum pressure occurs at zero flow rate. Also due to increase in M , ϵ and W_e pressure rise increases. The pumping regions, peristaltic pumping ($\theta > 0$ and $P' > 0$), augmented pumping ($\theta > 0$ and $P' < 0$) and retrograde pumping ($\theta < 0$ and $P' > 0$) are also shown in *Figs.* It become obvious that pumping region become wider

as M , W_e and ϵ increase. In *Fig. 2.8 – 2.13* friction forces for inner and outer wall versus flow rate are described. These forces possess opposite behaviour to that of pressure gradient where as inner friction force behaves similar to outer friction force for the same values of parameters, moreover outer friction is larger than inner friction force for same value of parameters.

2.6.2 Magnetic Field Characteristics

The distribution of axial induced magnetic field h_z at line $r = 0.22$ and for other fixed set of parameters with different values of M along axial coordinates z is displayed in *Fig. 2.14*. It can be seen that by increasing the Hartmann number M the axial induced magnetic field h_z also increases. In *Fig. 2.15*, the effects of volume flow rate θ on axial induced magnetic field is shown. It is observed that axial induced magnetic field h_z increases as volume flow increases and similar behaviour is seen for magnetic Reynolds number R_m in *Fig. 2.16*.

The *Figs. 2.17 to 2.20* present the variation of axial induced magnetic field h_z across the annulus for several values of θ , M and R_m . By increasing the Hartmann number M , the axial induced magnetic field h_z first decreases in region $[0, 0.5]$ and then it increases in region $[0.5, 1]$ and it is shown in *Fig. 2.17*. The graphical results shown in *Fig. 2.18*, present that an increase in magnetic Reynolds number R_m results in an increase in the magnitude of axial induced magnetic field h_z . The graphical results shown in *Fig. 2.19*, present that an increase in volume flow rate θ results in an increase in the magnitude of axial induced magnetic field h_z . *Fig. 2.20* depicts the effect of Weissenberg number W_e on h_z . Clearly an increase in W_e is followed by an decrease in axial induced magnetic field h_z in region $[0, 0.5]$ and then it increases in region $[0.5, 1]$.

The variation of the current density J_o at the inlet of annulus i.e. at $z = 0$, for different values of Hartmann number M and magnetic Reynolds number R_m is observed in *Figs. 2.21 and 2.22*. It is observed that increase in both M and R_m results in increase of current density.

2.6.3 Fluid Trapping

Trapping is the phenomena in which an internal circulating bolus of the fluid by closed streamline is formed and this bolus is pulled forward along with the peristaltic wave. Effects of Hartmann number M and radius ratio ϵ are shown in *Figs. 2.23 and 2.24*.

In *Fig. 2.23*, the effect of Hartmann number M on trapping is shown, it is seen that the volume of the bolus increases with increasing value of Hartmann number M . It is also observed that as M increases more trapped bolus appear. Similar behaviour is observed for the variation of ϵ in *Fig. 2.24*.

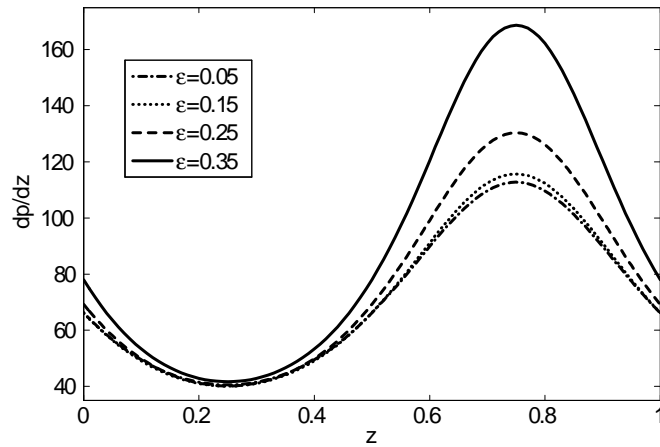


Fig. 2.2: The variation of pressure gradient dp/dz with z for different values of ϵ at $\theta = -0.121$, $\alpha = 0.13$, $M = 2$, $n = 0.3$ and $W_e = 0.16$.

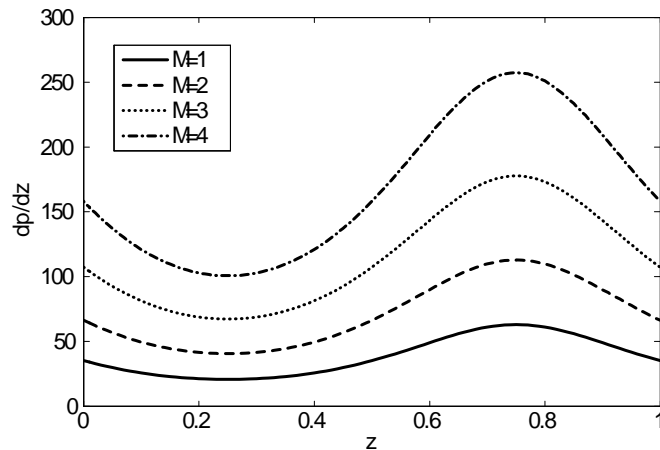


Fig. 2.3: The variation of pressure gradient dp/dz with z for different values of M at $\theta =$

-0.121 , $\alpha = 0.13$, $\epsilon = 0.01$, $n = 0.3$ and $W_e = 0.162$.

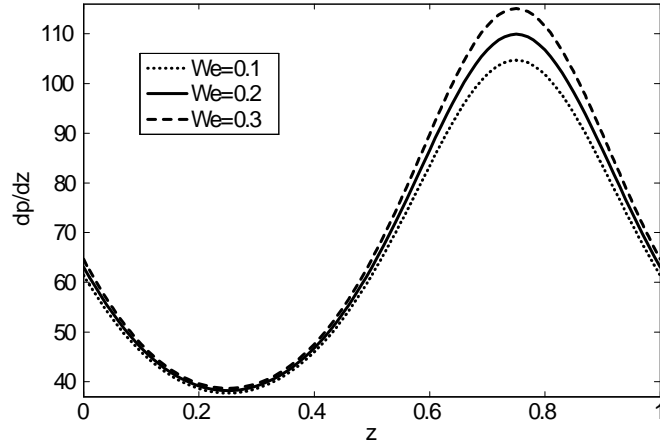


Fig. 2.4: The variation of pressure gradient dp/dz with z for different values of W_e at $\theta = -0.121$, $\alpha = 0.13$, $\epsilon = 0.1$, $n = 0.4$, $M = 2$.

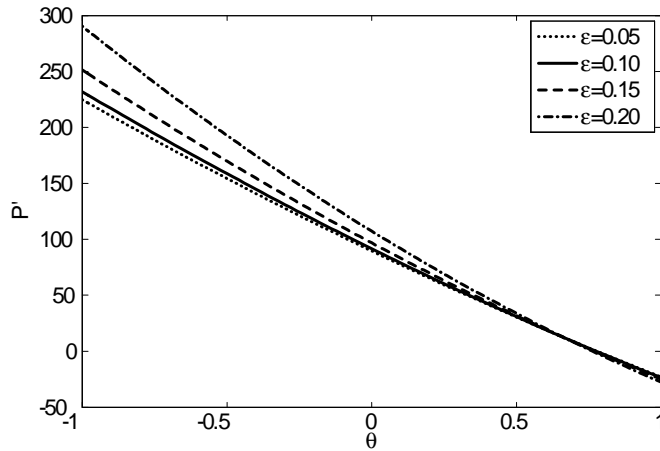


Fig. 2.5: The variation of pressure rise P' with θ for different values of ϵ at $\alpha = 0.3$, $n = 0.3$, $M = 2$ and $W_e = 0.162$.

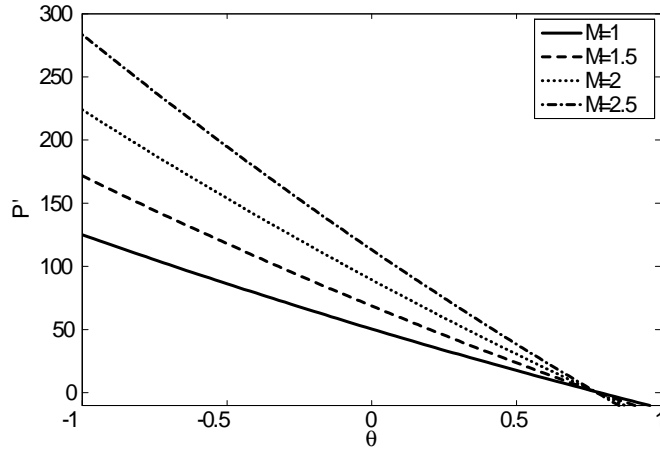


Fig. 2.6: The variation of pressure rise P' with θ for different values of M at $\alpha = 0.3$, $n = 0.3$, $\epsilon = 0.01$ and $W_e = 0.162$.

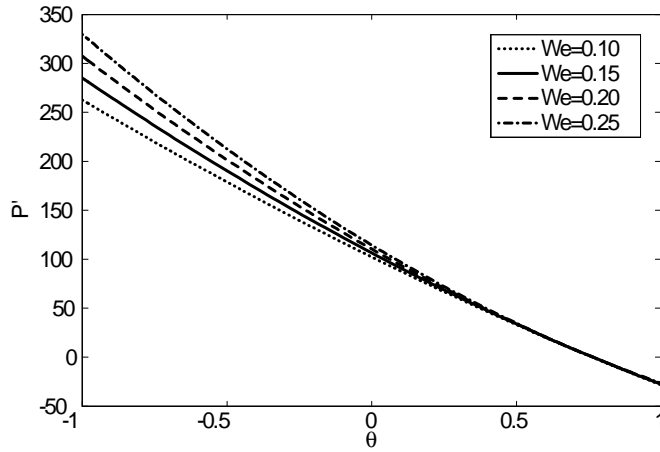


Fig. 2.7: The variation of pressure rise P' with θ for different values of W_e at $\alpha = 0.3$, $n = 0.3$, $M = 2$ and $\epsilon = 0.2$.

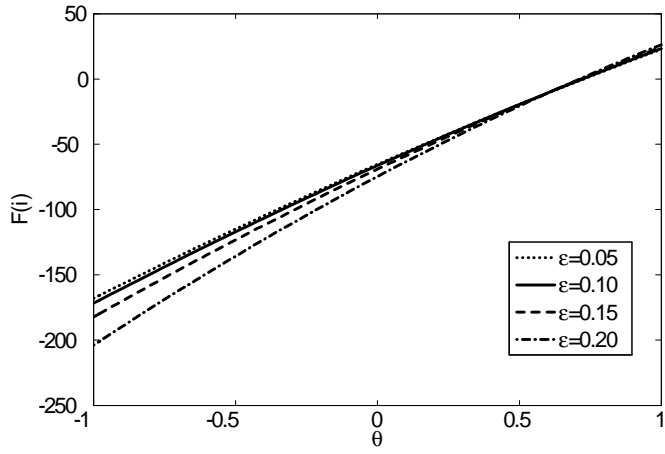


Fig. 2.8: The variation of friction force $F(i)$ (on outer wall) with θ for different values of ϵ at $\alpha = 0.3$, $n = 0.3$, $M = 2$ and $W_e = 0.162$.

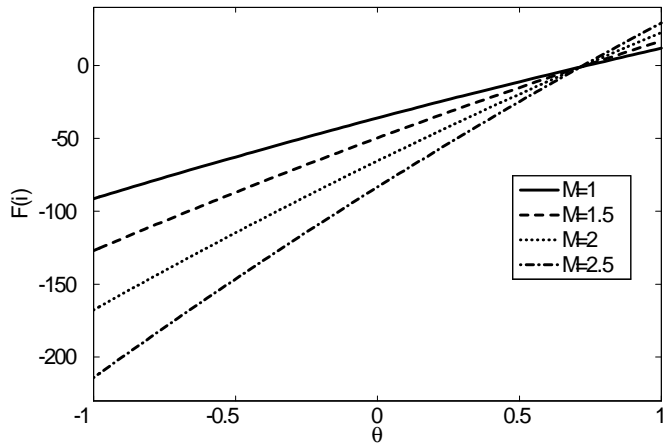


Fig. 2.9: The variation of friction force $F(i)$ (on outer wall) with θ for different values of M at $\alpha = 0.3$, $n = 0.3$, $M = 2$ and $W_e = 0.162$.

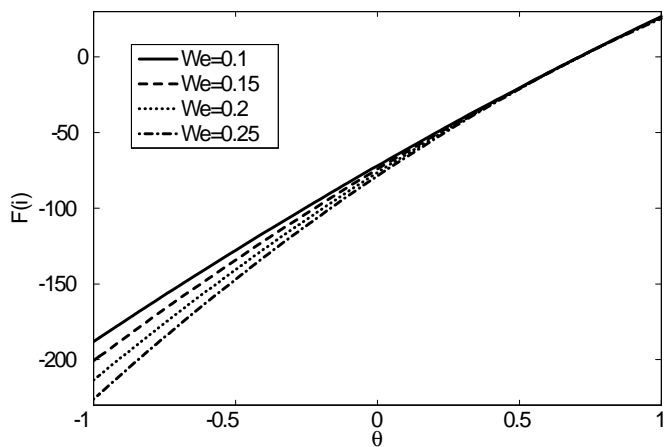


Fig. 2.10: The variation of friction force $F(i)$ (on outer wall) with θ for different values of We at $\alpha = 0.3$, $n = 0.3$, $M = 2$ and $\epsilon = 0.2$.

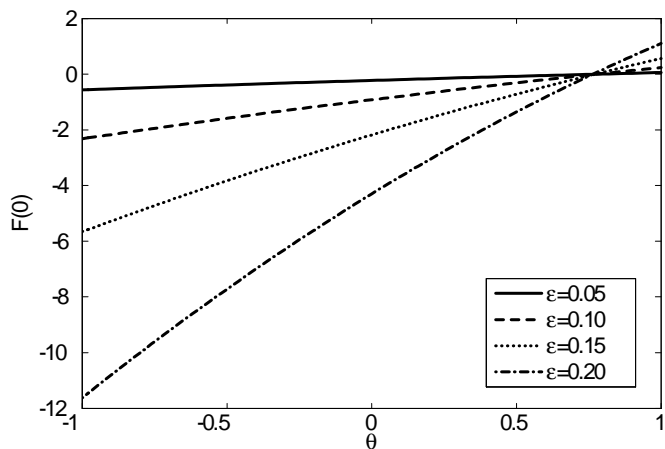


Fig. 2.11: The variation of friction force $F(i)$ (on outer wall) with θ for different values of ϵ at $\alpha = 0.3$, $n = 0.3$, $M = 2$ and $We = 0.162$.

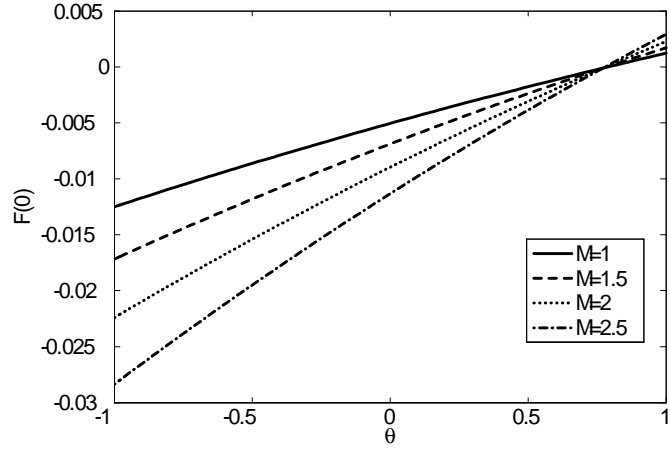


Fig. 2.12: The variation of friction force $F(i)$ (on outer wall) with θ for different values of M at $\alpha = 0.32$, $n = 0.3$, $\epsilon = 0.01$ and $W_e = 0.162$.

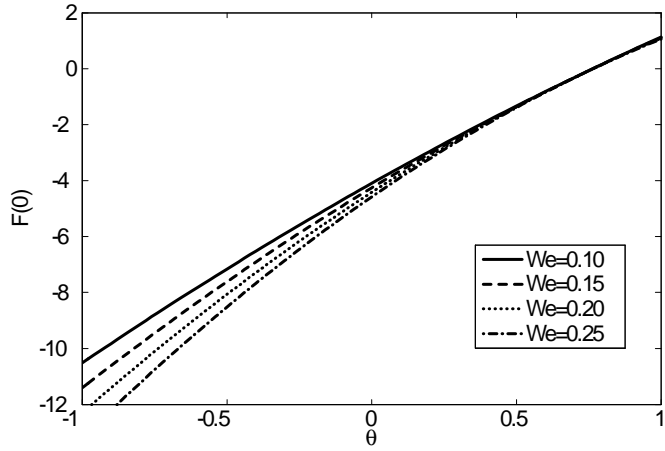


Fig. 2.13: The variation of friction force $F(i)$ (on outer wall) with θ for different values

of W_e at $\alpha = 0.3$, $n = 0.3$, $M = 2$ and $\epsilon = 0.02$.

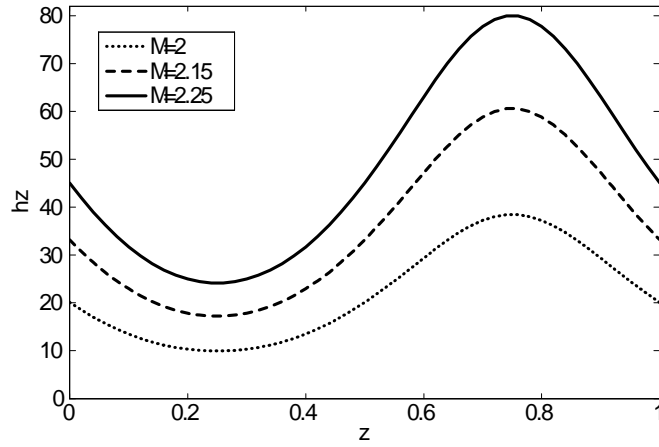


Fig. 2.14: The variation of axial induced magnetic field h_z with the axial coordinate z for different values of M at $\theta = -0.121$, $\alpha = 0.13$, $\epsilon = 0.25$, $R_m = 1$, $n = 0.99$ and $W_e = 0.162$ at $r = 0.22$.

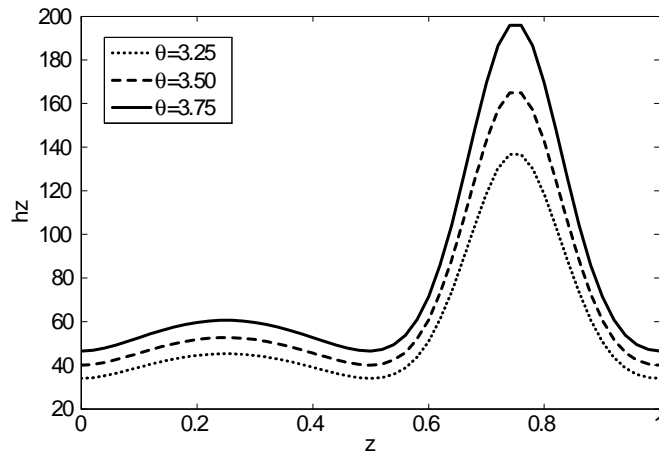


Fig. 2.15: The variation of axial induced magnetic field h_z with the axial coordinate z for different values of θ at $R_m = 1$, $\alpha = 0.3$, $\epsilon = 0.25$, $n = 0.99$, $M = 1.5$, $W_e = 0.162$ at $r = 0.22$.

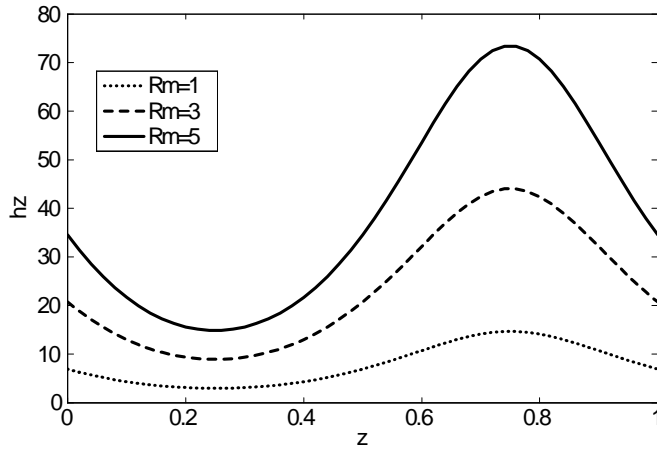


Fig. 2.16: The variation of axial induced magnetic field h_z with the axial coordinate z for different values of R_m at $\theta = -0.121$, $\alpha = 0.13$, $\epsilon = 0.25$, $M = 1.75$, $n = 0.99$, $W_e = 0.162$ at $r = 0.22$.

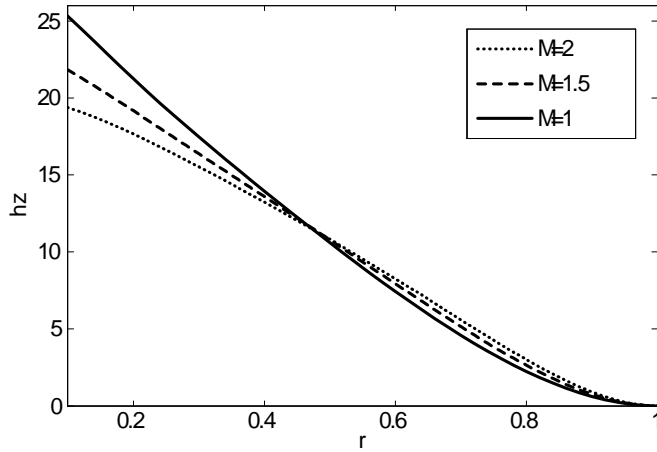


Fig. 2.17: The variation of axial induced magnetic field h_z across the annulus for $\theta = 0.3$, $\alpha = 0.3$, $\epsilon = 0.05$, $R_m = 3$, $n = 0.39$, $W_e = 0.2$ and $z = 0.5$ and different values of M where $r \in [\epsilon, r_2]$.

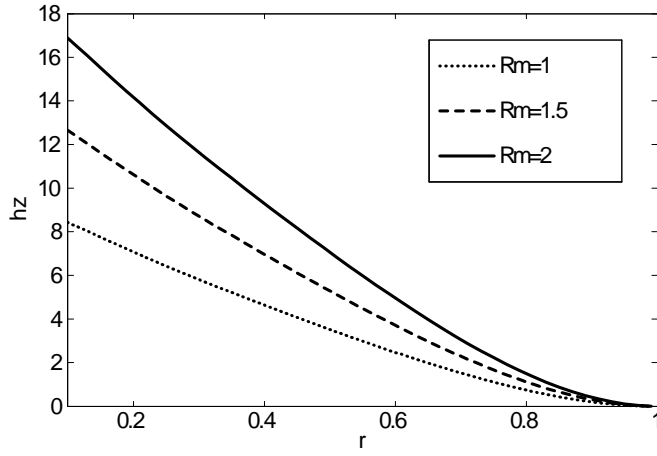


Fig. 2.18: The variation of axial induced magnetic field h_z across the annulus for $\theta = 0.5$, $\alpha = 0.2$, $\epsilon = 0.05$, $R_m = 0.5$ and $z = 0.4$ and different values of R_m where $r \in [\epsilon, r_2]$.

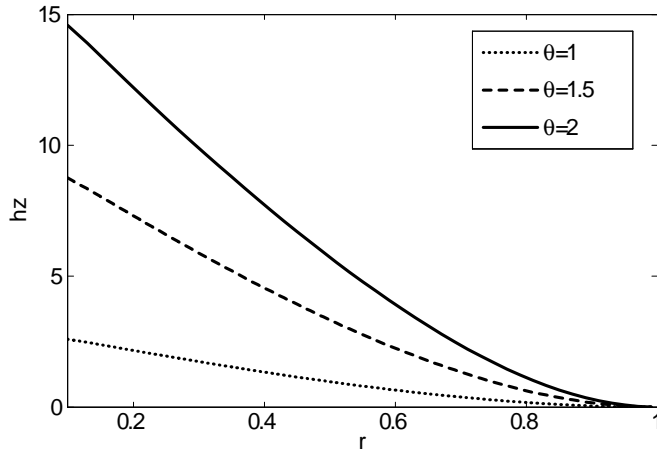


Fig. 2.19: The variation of axial induced magnetic field h_z across the annulus for $\theta = 0.5$, $\alpha = 0.2$, $\epsilon = 0.05$, $R_m = 0.5$, and $z = 0.4$ and different values of M where $r \in [\epsilon, r_2]$.

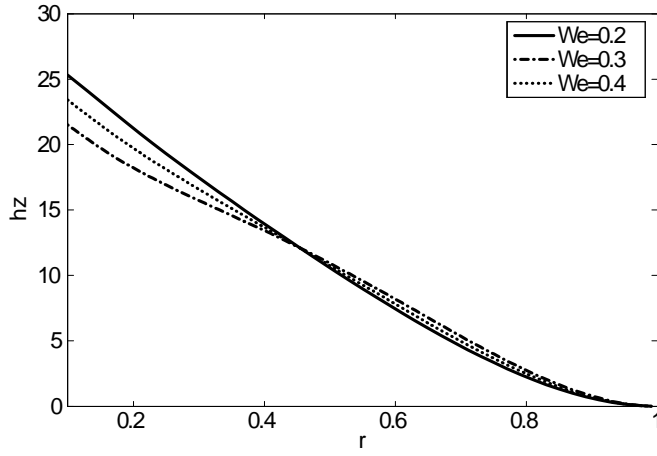


Fig. 2.20: The variation of axial induced magnetic field h_z across the annulus for $\theta = 0.5$, $\alpha = 0.2$, $\epsilon = 0.05$, $R_m = 0.5$ and $z = 0.4$ and different values of W_e where $r \in [\epsilon, r_2]$.

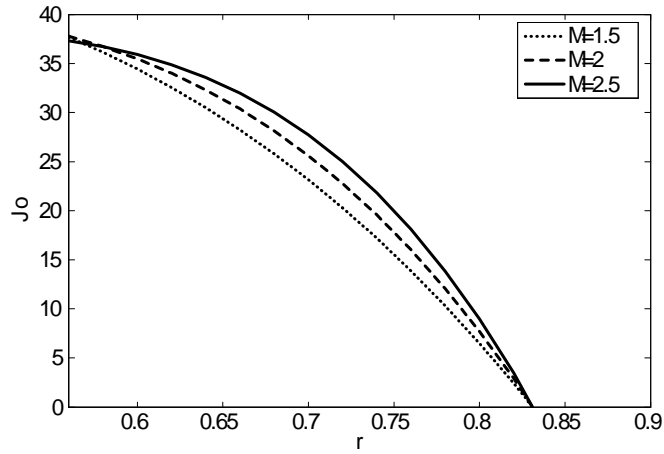


Fig. 2.21: The variation of current density J_o across the annulus for $\theta = 0.5$, $\alpha = 0.2$, $\epsilon = 0.05$, $R_m = 0.5$ and $z = 0.4$ and different values of M where $r \in [\epsilon, r_2]$.

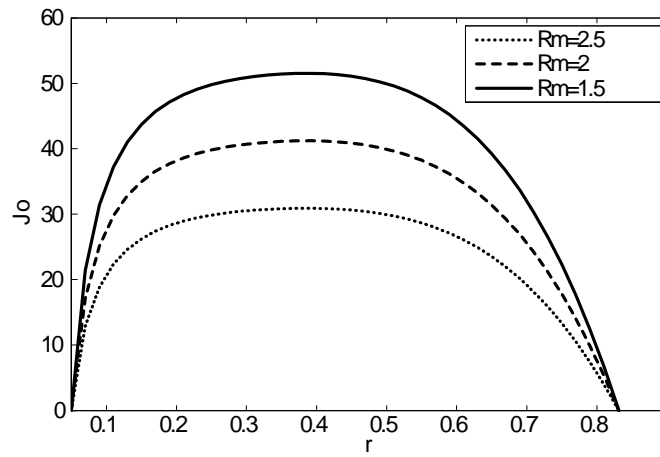
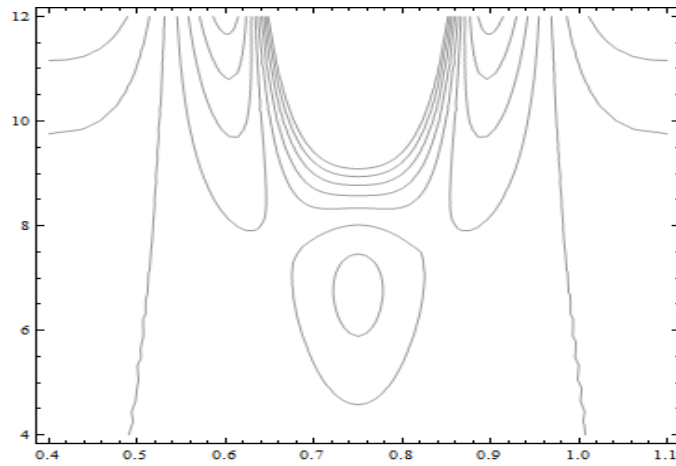
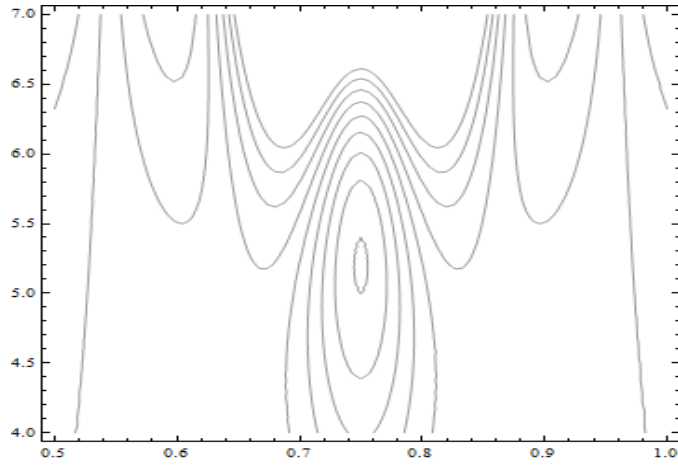


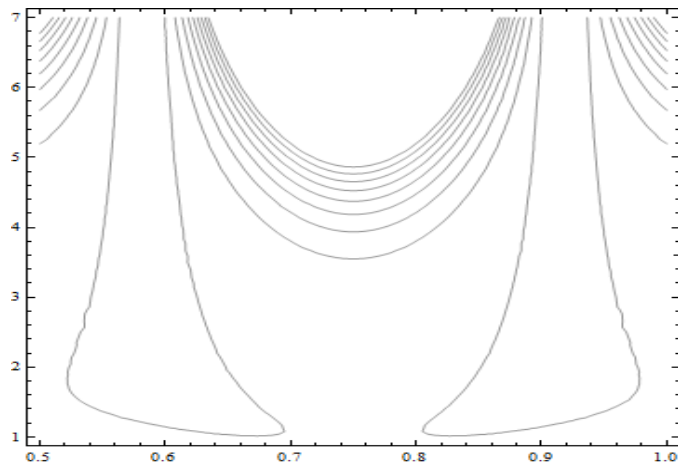
Fig. 2.22: The variation of current magnetic field J_o across the annulus for $\theta = 0.5$, $\alpha = 0.2$, $\epsilon = 0.05$, $M = 0.5$ and $z = 0.4$ and different values of R_m where $r \in [\epsilon, r_2]$.



(a)

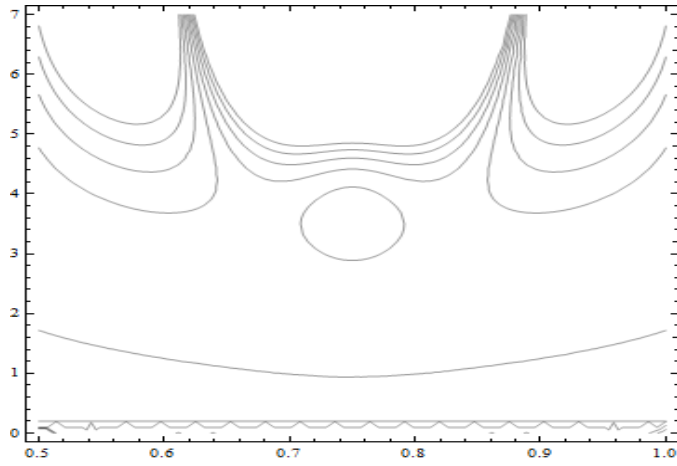


(b)

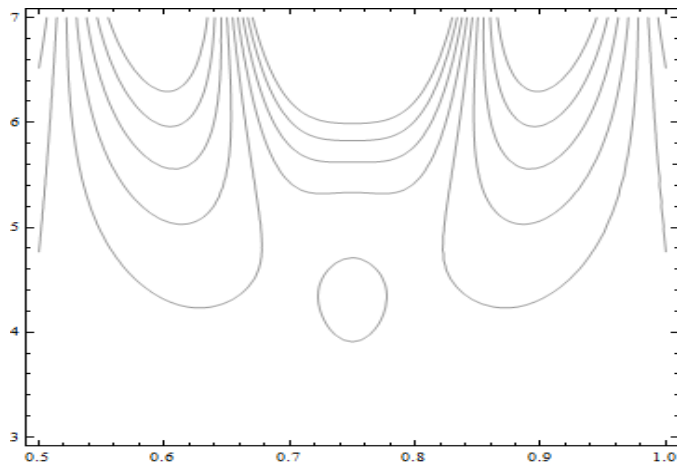


(c)

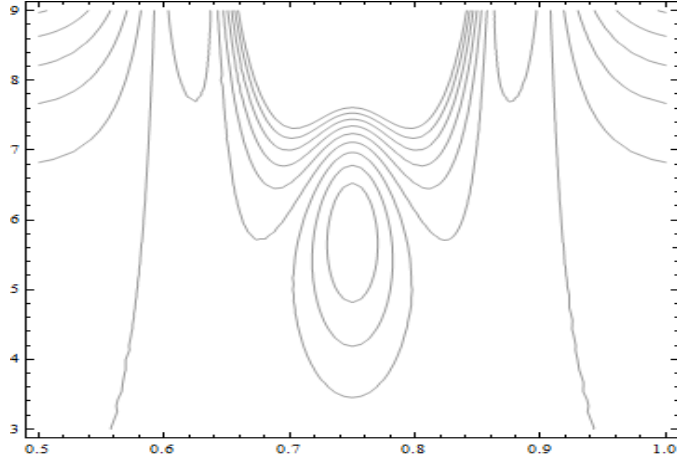
Fig. 2.23: Plot showing streamlines for different values of Hartmann number $M = 0.25, 1, 2$ (a, b, c respectively) for $\alpha = 0.3$, $\theta = 0.6$, $\epsilon = 0.4$ and $W_e = 0.16$ and $n = 0.6$.



(a)



(b)



(c)

Fig. 2.24 : Plot showing streamlines for different values of radius ratio $\epsilon = 0.2, 0.3, 0.5$.
(*a, b, c* respectively) for $\alpha = 0.3, \theta = 0.6, \epsilon = 0.4$ and $W_e = 0.4$ and $n = 0.6$.

2.7 Concluding Remarks

Peristaltic flow of hyperbolic tangent fluid through an annulus is studied theoretically under the effects of the induced magnetic field. The expressions for axial pressure gradient, current density, axial magnetic field and stream functions are obtained analytically. Graphical results are shown for pressure gradient, pressure rise per wavelength, frictional forces, axial induced magnetic field, current density and trapping. The main points of performed analysis are as follows

- (i) As the radius ratio and Weissenberg number increase, the maximum amplitude of pressure gradient increases.
- (ii) With increasing flow rate the pressure rise decreases i.e. there is an inverse relation between P' and θ .
- (iii) The behaviour of inner and outer frictional forces is opposite to the pressure rise.
- (iv) The axial induced magnetic field h_z increases along axial coordinates as Hartmann

number, Weissenberg number and magnetic Reynolds number increase.

(v) The axial induced magnetic field h_z increases across the annulus by increasing the magnetic Reynolds number and flow rate.

(vi) Current density and magnetic Reynolds number behave likely i.e. by increasing the magnetic Reynolds number, the current density also increases.

2.8 Appendix II

$$\begin{aligned}
b_1 &= \frac{r_1^2 r_2^k - r_1^k r_2^2}{r_1^k r_2^{-k} - r_1^{-k} r_2^k}, \quad b_2 = \frac{1}{4(1-n) - M^2 r_2^2}, \quad b_3 = \frac{r_1^2 r_2^{-k} - r_1^{-k} r_2^2}{r_1^{-k} r_2^k - r_1^k r_2^{-k}}, \quad b_4 = b_2 b_3, \quad b_5 = b_1 b_2, \\
b_6 &= \frac{(r_2^2 - r_1^2)}{2}, \quad b_7 = 2b_4 \frac{(r_2^{k+2} - r_1^{k+2})}{k+2} + 2b_5 \frac{(r_2^{-k+2} - r_1^{-k+2})}{-k+2} + 2b_2 \frac{(r_2^4 - r_1^4)}{4}, \\
b_8 &= \frac{1}{k^2(1-n) - M^2 r_2^2}, \quad b_9 = \frac{1}{(1-n)(2k-1)^2 - M^2 r_2^2}, \quad b_{10} = \frac{1}{(1-n)(2k+1)^2 - M^2 r_2^2}, \\
b_{11} &= \frac{1}{(1-n)9 - M^2 r_2^2}, \quad b_{12} = \frac{1}{(1-n) - M^2 r_2^2}, \quad b_{13} = \frac{1}{(1-n)(k+1)^2 - M^2 r_2^2}, \\
b_{14} &= \frac{1}{(1-n)(-k+1)^2 - M^2 r_2^2}, \quad b_{15} = kb_4 b_8, \quad b_{18} = kb_5 b_8, \quad b_{19} = 2b_2^2, \quad b_{20} = k(k-1)b_4 b_8, \\
b_{21} &= k(k+1)b_5 b_8, \quad b_{22} = 2b_2^2, \quad b_{23} = b_4 b_8, \quad b_{24} = b_5 b_8, \quad b_{25} = b_2^2, \quad b_{26} = k^2 b_4^2 b_9, \\
b_{27} &= k^2 b_5^2 b_{10}, \quad b_{28} = 4b_2^2 b_{11}, \quad b_{29} = 2k^2 b_4 b_5 b_{12}, \quad b_{30} = 4kb_2 b_4 b_{13}, \quad b_{31} = 4kb_2 b_5 b_{14}, \\
b_{32} &= k^2(k-1)b_4^2 b_9, \quad b_{33} = k^2(k+1)b_5^2 b_{10}, \quad b_{34} = 2kb_2 b_5 b_{14}, \quad b_{35} = k^2(k-1)b_4 b_5 b_{12}, \\
b_{36} &= k^2(k+1)b_5^2 b_{10}, \quad b_{37} = 2kb_2 b_5 b_{14}, \quad b_{38} = 2k(k-1)b_2 b_4 b_{13}, \quad b_{39} = 2k(k+1)b_2 b_5 b_{14}, \\
b_{40} &= 4b_2^2 b_{11}, \quad b_{41} = -(1-n) \frac{\partial p_o}{\partial z} b_{17} - (1-n) \frac{\partial p_o}{\partial z} b_{20} + M^2 r_2^2 \frac{\partial p_o}{\partial z} b_{23}, \\
b_{42} &= (1-n) \frac{\partial p_o}{\partial z} b_{18} - (1-n) \frac{\partial p_o}{\partial z} b_{21} + M^2 r_2^2 \frac{\partial p_o}{\partial z} b_{24}, \\
b_{43} &= -(1-n) \frac{\partial p_o}{\partial z} b_{19} - (1-n) \frac{\partial p_o}{\partial z} b_{22} + M^2 r_2^2 \frac{\partial p_o}{\partial z} b_{25}, \\
b_{44} &= -nW_e \left(\frac{\partial p_o}{\partial z} \right)^2 b_{26} - 2nW_e \left(\frac{\partial p_o}{\partial z} \right)^2 b_{32}, \quad b_{45} = -nW_e \left(\frac{\partial p_o}{\partial z} \right)^2 b_{27} + 2nW_e \left(\frac{\partial p_o}{\partial z} \right)^2 b_{36}, \\
b_{46} &= -nW_e \left(\frac{\partial p_o}{\partial z} \right)^2 b_{28} - 2nW_e \left(\frac{\partial p_o}{\partial z} \right)^2 b_{40}, \quad b_{47} = [nW_e b_{29} - 2nW_e (b_{33} - b_{35})] \left(\frac{\partial p_o}{\partial z} \right)^2, \\
b_{48} &= [-nW_e b_{30} - 2nW_e b_{34} - 2nW_e b_{38}] \left(\frac{\partial p_o}{\partial z} \right)^2, \\
b_{49} &= \left(\frac{\partial p_o}{\partial z} \right)^2 [nW_e b_{31} + 2nW_e b_{37} - 2nW_e b_{39}], \quad b_{50} = b_2 \left(\frac{r_1^2 r_2^k - r_1^k r_2^2}{r_1^{-k} r_2^k - r_1^k r_2^{-k}} \right), \\
b_{51} &= b_{42} + \frac{1}{r_1^{-k} r_2^k - r_1^k r_2^{-k}} [b_{43} (r_1^2 r_2^k - r_1^k r_2^2) + b_{44} (r_1^{2k-1} r_2^k - r_1^k r_2^{2k-1}) + b_{45} (r_1^{-(2k+1)} r_2^k - r_1^k r_2^{-(2k+1)}) \\
&\quad b_{46} (r_1^3 r_2^k - r_1^k r_2^3) + b_{47} (r_1^{-1} r_2^k - r_1^k r_2^{-1}) + b_{48} (r_1^{k+1} r_2^k - r_1^k r_2^{k+1}) + b_{49} (r_1^{-k+1} r_2^k - r_1^k r_2^{-k+1})], \\
b_{52} &= b_2 \left(\frac{r_1^2 r_2^{-k} - r_1^{-k} r_2^2}{r_1^k r_2^{-k} - r_1^{-k} r_2^k} \right), \quad b_{53} = b_{41} + \frac{1}{r_1^{-k} r_2^k - r_1^k r_2^{-k}} [b_{43} (r_1^2 r_2^{-k} - r_1^{-k} r_2^2) \\
&\quad + b_{44} (r_1^{2k-1} r_2^{-k} - r_1^{-k} r_2^{2k-1}) + b_{45} (r_1^{-(2k+1)} r_2^{-k} - r_1^{-k} r_2^{-(2k+1)})]
\end{aligned}$$

$$\begin{aligned}
& +b_{46} \left(r_1^3 r_2^{-k} - r_1^{-k} r_2^3 \right) + b_{47} \left(r_1^{-1} r_2^{-k} - r_1^{-k} r_2^{-1} \right) + b_{48} \left(r_1^{k+1} r_2^{-k} - r_1^{-k} r_2^{k+1} \right) \\
& + b_{49} \left(r_1^{-k+1} r_2^{-k} - r_1^{-k} r_2^{-k+1} \right) \Big], \\
b_{54} & = b_{41} - b_{53}, \quad b_{55} = b_{42} - b_{51}, \\
b_{56} & = 2 \left[-b_{52} \left(\frac{r_2^{k+2} - r_1^{k+2}}{k+2} \right) - b_{50} \left(\frac{r_2^{-k+2} - r_1^{-k+2}}{-k+2} \right) + b_2 \left(\frac{r_2^4 - r_1^4}{4} \right) \right], \\
b_{57} & = 2 \left[b_{44} \left(\frac{r_2^{2k+1} - r_1^{2k+1}}{2k+1} \right) + b_{45} \left(\frac{r_2^{-2k+1} - r_1^{-2k+1}}{-2k+1} \right) + b_{46} \left(\frac{r_2^5 - r_1^5}{5} \right) + b_{47} (r_2 - r_1) \right. \\
& + b_{48} \left(\frac{r_2^{k+3} - r_1^{k+3}}{k+3} \right) + b_{49} \left(\frac{r_2^{-k+3} - r_1^{-k+3}}{-k+3} \right) + b_{54} \left(\frac{r_2^{k+2} - r_1^{k+2}}{k+2} \right) + b_{55} \left(\frac{r_2^{-k+2} - r_1^{-k+2}}{-k+2} \right) \\
& \left. + b_{43} \left(\frac{r_2^4 - r_1^4}{4} \right) \right], \\
b_{58} & = \frac{1}{b_7} + \frac{1}{b_{56}}, \quad b_{59} = \frac{b_6}{b_7} - \frac{b_{57}}{b_{56}}.
\end{aligned}$$

Bibliography

- [1] Y. Abd elmaboud, Influence of induced magnetic field on peristaltic flow in an annulus, *Comm Nonlinear Sci Numb Simu.* 17(2012) 685 – 698.
- [2] A. H. Shapiro, M. Y. Jafferin, S. L. Weinberg, Peristaltic pumping with long wavelengths at low Reynolds number, *J. Fluid Mech.* 35(1969)669.
- [3] Y. C. Fung, C. S. Yih, Peristaltic transport, *J. Appl. Mech.* 35(1968)669.
- [4] J. C. Burns, T. Parkes, Peristaltic motion, *J. Fluid Mech.* 29(1967)731.
- [5] M. H. Haroun, Effect of Deborah number and phase difference on peristaltic transport of a third order fluid in an asymmetric channel, *Commun Nonlinear Sci Numer Simulat.* 4(2007) 463
- [6] C. Barton, S. Raynor, Peristaltic flow in tubes, *Bull. Math. Biophys.* 30(1968)663.
- [7] T. W. Latham, Fluid motion in a peristaltic pump, MS. Thesis, Massachusetts Institute of Technology, Cambridge, 1966.
- [8] S. U. S. Choi, Enhancing thermal conductivity of fluids with nanoparticles, in: D. A. Siginer, H.P. Wang (Eds.), *Developments and Applications of Non-Newtonian Flows*, ASME, New York. 66 (1995) 99 – 105.
- [9] P. Rana and R. Bhargava, Flow and heat transfer of a nanofluid over a nonlinearly stretching sheet: A numerical study, *Comm. Nonlinear Sci. Num. Simul.* DOI : 10.1016/j.cnsns.2011.05.009.

- [10] N. S. Akbar and S. Nadeem, Endoscopic effects on the peristaltic flow of a nanofluid, *Commun. Theor. Phys.* 56(2011)761.
- [11] N. S. Akbar, S. Nadeem, T. Hayat and A. A. Hendi, Peristaltic flow of a nanofluid in a non-uniform tube, *Heat and Mass Transfer.* 48(2012)451.
- [12] M. Ealshahed and M. H. Haroun, Peristaltic transport of Johnson-Segalman fluid under effect of a magnetic field, *Math. Prob in Eng.* 6(2005)663.
- [13] J. Buongiorno, Convective Transport in Nanofluids. *Journal of Heat Transfer (American Society Of Mechanical Engineers).* 128(3) (2010) 240.
- [14] Kh. S. Mekheimer, Y. Abd Elmaboud, Peristaltic flow of a couple stress fluid in an annulus; Application of an endoscope, *Physica A.* 387(2008)2403.
- [15] J. H. He, Application of homotopy perturbation method to nonlinear wave equations, *Chaos, Solitons & Fractals.* 26(2005)695.
- [16] A. M. Siddiqui, A. Zeb, Q. K. Ghori and A. M. Benharbit, Homotopy perturbation method for heat transfer flow of a third grade fluid between parallel plates, *Chaos Solitons and Fractals.* 36 (2008) 182 – 192.
- [17] N. S. Akbar, S. Nadeem, T. Hayat and A. A. Hendi, Effects of heat and mass transfer on the peristaltic hyperbolic tangent fluid in an annulus, *Int. J. of Heat and Mass Transfer.* 54(2011)4360 – 4369.
- [18] S. Nadeem and N. S. Akbar, Series solutions for the peristaltic flow of a Tangent hyperbolic fluid in a uniform inclined tube, *Zeitschrift fur Naturforschung,* 65a(2010)887.